

# Development of Countermeasure Strategies for Protecting Bridge Girders against Over-height Vehicles Impact

Interim Report 1: Literature Review

Revision B

April 8, 2024

Prepared for:  
Federal Highway Administration  
Office of Bridges and Structures – HIBS-10  
1200 New Jersey, Ave, SE  
Washington, DC 20590

Prepared by:  
Robert T. Bocchieri<sup>1</sup>  
Jessica Reese<sup>1</sup>  
Brett Commander<sup>2</sup>  
William Williams<sup>3</sup>

<sup>1</sup>Applied Research Associates, Inc.

<sup>2</sup>Bridge Diagnostics, Inc

<sup>3</sup>Texas A&M Transportation Institute

Contract No. 693JJ323D000001

Requisition No. HIF220029PR

ARA Project No. D00335

## Table of Contents

<b>1. Introduction.....</b>	<b>1</b>
<b>2. Energy Absorbing Systems for Protecting Bridge Girders.....</b>	<b>3</b>
2.1. PC Girder Protection with CFRP Wrap and Honeycomb Energy Absorber .....	3
2.1.1. System Description .....	3
2.1.2. Inspection and Monitoring Considerations.....	6
2.2. Steel Girder Protection with Sorbothane® High-Impact Rubber .....	7
2.2.1. System Description .....	7
2.2.2. Inspection and Monitoring Considerations.....	8
2.3. RC Girder Protection with I-Lam Impact Laminate .....	10
2.3.1. Systems Description.....	10
2.3.2. Installation and Performance on ODOT Bridge .....	13
2.3.3. Inspection and Monitoring Considerations.....	15
2.4. Steel Railroad Bridge Protection Using Energy Absorbing Steel Crash Beams .....	16
2.4.1. System Description .....	16
2.4.2. Inspection and Monitoring Considerations.....	21
2.5. Concrete Box-Girder Protection with Stiff Guards Backed with Polyurethane Foam .....	22
2.5.1. System Description .....	22
2.5.2. Inspection and Monitoring Considerations.....	24
<b>3. Other Protection Methods.....</b>	<b>26</b>
3.1. Bridge Protective Beam Wrap .....	26
3.2. Hybrid Composite Beam.....	28
<b>4. Over-height Collision Impact Loading and Analysis Methods .....</b>	<b>33</b>
4.1. Bridge Impact Loading Specified in Industry Standards.....	33
4.2. Peak and Average Impact Force from a Box Truck Impact on a PC Box Girder.....	35
4.3. Demand Model for Varied Stiffness Cargo on a Semi-Trailer Truck .....	37
4.4. Demand Equation for Varied Impactors on AASHTO Bridge Girders.....	39
4.5. Analytical Design Methods Using Crushable Sandwich Structures.....	41
4.6. Computational Methods.....	44
4.6.1. FEA Models of Vehicles Used for Analysis of Over-height Impact Events .....	44
4.6.2. Materials Modeling.....	47
<b>5. References .....</b>	<b>49</b>

## List of Figures

Figure 1. CFRP wrapping of prestressed concrete girders (Agrawal, El-Tawil, Cao, & Wong, 2022).....	3
Figure 2. Simulation of a concrete bridge with CFRP wrap on the front girder subject to impact with a trailer (Agrawal, El-Tawil, Cao, & Wong, 2022). ....	3
Figure 3. Simulation of a concrete bridge with honeycomb attached on the front girder subject to impact with a trailer (Agrawal, El-Tawil, Cao, & Wong, 2022). ....	4
Figure 4. Drop-hammer test of PC beam with honeycomb (Agrawal, El-Tawil, Cao, & Wong, 2022).....	4
Figure 5. Deformation of the beam from drop-hammer impact at 10 mph with (a) no honeycomb (b) with honeycomb (Agrawal, El-Tawil, Cao, & Wong, 2022). ....	5
Figure 6. Deformation of the beam from drop-hammer impact at 20 mph with (a) no honeycomb (b) with honeycomb (Agrawal, El-Tawil, Cao, & Wong, 2022). ....	5
Figure 7. Strain in impact beam from drop-hammer tests (a) at 10 mph and (b) at 20 mph (Agrawal, El-Tawil, Cao, & Wong, 2022). ....	5
Figure 8. Bridge and I-girder cross section (Aly & Hoffmann, 2022).....	7
Figure 9. Over-height vehicle selected for analysis (Aly & Hoffmann, 2022). ....	7
Figure 10. Vehicle-girder impact Ansys analysis 70 mph (113 km/h) (Aly & Hoffmann, 2022).....	9
Figure 11. Double-layer I-Lam sandwich system for collision protection (Cheng & Qiao, 2015). ....	10
Figure 12. Final installed I-Lam panel on bridge DEL-23-12.99 (Qiao P. , Yang, Mosallam, & Song, 2008).....	11
Figure 13. Geometry of the RC beam used in impact testing of the I-Lam (Cheng & Qiao, 2015). ....	11
Figure 14. Impact test set-up of the RC beam impacted with a wooden impactor (Qiao P. , Yang, Mosallam, & Song, 2008). ....	12
Figure 15. I-Lam panel after impact (Cheng & Qiao, 2015).....	12
Figure 16. Tensile damage of the RC after impact (Cheng & Qiao, 2015).....	13
Figure 17. Details of the original I-Lam installation (Qiao P. , Yang, Mosallam, & Song, 2008).....	14
Figure 18. Schematic of I-Lam installed along the bottom of a RC girder (Qiao P. , Yang, Mosallam, & Song, 2008). ....	15
Figure 19. Typical through plate girder railroad bridge over a highway overpass (Xu, et al., 2022).....	17
Figure 20. Schematic of (a) TPG steel bridge with a crash beam attached and (b) attachment details (Xu, et al., 2022). ....	17
Figure 21. Crash beam test articles (Xu, et al., 2022). ....	18
Figure 22. Installation details for the crash beams using bolted C-channel supports (mm) (Xu, et al., 2022). ....	18

Figure 23. Testing frame (a) loading frame with scaled girder (Ozadagli, Moreu, Xu, & Wang, 2020) (b) test frame schematic (c) complete test setup with impact block (Xu, et al., 2022). .....	19
Figure 24. Crash beam configurations (Ozadagli, Moreu, Xu, & Wang, 2020).....	19
Figure 25. Test instrumentation (Xu, et al., 2022). .....	21
Figure 26. Sketch of bridge bumper to protect a box-girder (Sharma, Hurlebaus, & Gardoni, 2008).....	22
Figure 27. Experimental setup for impact testing of the bridge bumper (Sharma, Hurlebaus, & Gardoni, 2008). .....	23
Figure 28. Stress-strain for four EAM tested (Sharma, Hurlebaus, & Gardoni, 2008). .....	23
Figure 29. Example beam for over-height vehicle protection (Cao, et al., 2023).....	26
Figure 30. Bridge Protective Beam Wrap – Bridge Elevation (Smith, 2014).....	27
Figure 31. Bridge Protective Beam Wrap – Girder cross sections (Smith, 2014).....	27
Figure 32. Bridge beam hit with BPBW installed (Smith, 2014).....	28
Figure 33. Damage of the CFRP wrapped girder from over-height impact (Agrawal, El-Tawil, Cao, & Wong, 2022).....	28
Figure 34. Hybrid composite beam (Hillman, 2012).....	29
Figure 35. Cross section of PC girder (Jing, 2017). .....	29
Figure 36. Full-scale lateral impact test setup (Jing, 2017).....	30
Figure 37. Full-scale lateral impact test article with HCB shown (Jing, 2017).....	30
Figure 38. Full-scale lateral impact test article with PC girder shown (Jing, 2017).....	30
Figure 39. PC girder after the impact test (Jing, 2017).....	31
Figure 40. HCB girder after the impact test (Jing, 2017).....	32
Figure 41. Typical impact damage from over-height collisions (Harries, Kasan, Miller, & Brinkman, 2012).....	33
Figure 42. Reduction in static design forces accounting for bridge deck clearance (CEN, 2006). .....	34
Figure 43. Finite Element Model of the Truck Impactor (Jing, Zhang, Zhou, Zhao, & Li, 2023). .....	35
Figure 44. Proposed impact force demand model (a) ramped pulse for the soft case (b) triangular pulse for the semi-rigid and rigid case (Cao, et al., 2023).....	38
Figure 45. Loading application of the demand model (Cao, et al., 2023). .....	38
Figure 46. Types of impactors used in (a) concrete conduit pipe, (b) cylindrical steel tank, (c) PVC pipe, (d) wooden box container, (e) tractor semi-trailer (Oppong, Saini, & Behrouz, 2021).....	39
Figure 47. Impact force history on AASHTO girders from collisions with (a) concrete pipe (b) steel tank (c) PVC pipe (d) wooden box (e) tractor-semitrailer (Oppong, Saini, & Behrouz, 2021). .....	40
Figure 48. Impact force time history for various sizes of impacting objects traveling at a velocity of 120 km/h (75 mph): (a),(b) concrete pipe (c),(d) steel tank into Type I and Type IV girders (Oppong, Saini, & Behrouz, 2021).....	41

**Figure 49. Free-body diagram of the shear-off of an over-height portion of a truck (Qiao, Yang, & Mosallam, 2004). .....42**

**Figure 50. Discrete model of rigidly supported sandwich beam under impact (Qiao, Yang, & Mosallam, 2004). .....42**

**Figure 51. Example FEA model of RC box girder for over-height vehicle impact analysis (Jing, Zhang, Zhou, Zhao, & Li, 2023).....47**

## List of Tables

<b>Table 1. Summary of Energy Absorbing Bridge Girder Protection Systems .....</b>	<b>1</b>
<b>Table 2. Inspection and Instrumentation Methods – Honeycomb Energy Absorber on PS/C.....</b>	<b>6</b>
<b>Table 3. Inspection and Instrumentation Methods – Sorbothane® on Steel .....</b>	<b>8</b>
<b>Table 4. Comparisons of the maximum reaction forces due to impact (Cheng &amp; Qiao, 2015).....</b>	<b>13</b>
<b>Table 5. Inspection and Instrumentation Methods – I-Lam Impact Laminate .....</b>	<b>16</b>
<b>Table 6. Attenuation (%) of total bridge girder displacements (Ozadagli, Moreu, Xu, &amp; Wang, 2020).....</b>	<b>20</b>
<b>Table 7. Residual deformation and attenuation (%) of bridge girder displacements (Xu, et al., 2022).....</b>	<b>21</b>
<b>Table 8. Inspection and Instrumentation Methods – Steel Crash Beam .....</b>	<b>22</b>
<b>Table 9. Simulated Performance of the Bridge Bumper Using Different EAM with the 67g Impactor (Sharma, Hurlebaus, &amp; Gardoni, 2008). .....</b>	<b>24</b>
<b>Table 10. Inspection and Instrumentation Methods.....</b>	<b>25</b>
<b>Table 11. Indicative equivalent static design forces due to impact on superstructures (CEN, 2006). .....</b>	<b>34</b>
<b>Table 12. Varied Conditions for the Parametric Analysis from (Jing, Zhang, Zhou, Zhao, &amp; Li, 2023) .....</b>	<b>35</b>
<b>Table 13. Influence of Individual Parameters on Over-height Vehicle Collision (Jing, Zhang, Zhou, Zhao, &amp; Li, 2023) .....</b>	<b>36</b>
<b>Table 14. Fit Parameters to the Impact Force Formula (Note if the impact angle is zero, then d, e, and f are set to zero.).....</b>	<b>37</b>
<b>Table 15. Examples for Representative Tractor Semi-trailer Types (Cao, et al., 2023) .....</b>	<b>37</b>
<b>Table 16. Parameters used in the linear elastic analytical model (Qiao, Yang, &amp; Mosallam, 2004). .....</b>	<b>43</b>
<b>Table 17. Design Criterion for Protective Sandwich Structures (Yang &amp; Qiao, 2010), (Yang M. , 2006).....</b>	<b>44</b>
<b>Table 18. Examples of cargo types used with model #1 (Cao, et al., 2023).....</b>	<b>45</b>
<b>Table 19. FEA Vehicle or Cargo Models used for Bridge Girder Impact Analysis. ....</b>	<b>46</b>

## Revision Table

<b>Revision</b>	<b>Date</b>	<b>Revised Sections and Description of Changes</b>
A	1/31/2024	Initial Release
B	4/8/2024	All sections. Accepted all tracked changes and made revisions per comments as detailed in the document 'Combined Comments_FORM_Interim_Report_1_1Mar2024_ARA Responses.xlsx'

## 1. Introduction

An extensive review of the literature identified five energy absorbing (EA) systems that were proposed, tested, or analyzed for over-height vehicle bridge girder impact protection at various levels of development. These are summarized in Table 1. The EA methodologies used include plastic deformation of steel components and crushing of honeycomb, rubber, or foams. In most cases, scaled tests were performed to demonstrate performance. No full-scale testing was performed on any system and only one system was installed (I-Lam, EA System #3) on a bridge in service but has been subsequently removed due to debonding issues. Besides protection beams that are not designed to absorb energy, we did not discover any other systems installed on highway bridges in the United States and other countries during our literature search. Finite element analysis (FEA) of most of the systems were performed as part of the design process. Cost information for manufacture and installation was not available for any system. Section 2 outlines each approach in greater detail. Section 3 includes other protection methods that have the potential to be used in coordination with energy absorbing approaches.

*Table 1. Summary of Energy Absorbing Bridge Girder Protection Systems*

EA System	Author(s)	Development Status
1. PC Girder Protection with carbon fiber reinforced polymer (CFRP) Wrap and Honeycomb Energy Absorber	<ul style="list-style-type: none"> <li>(Agrawal, El-Tawil, Cao, &amp; Wong, 2022)</li> </ul>	<ul style="list-style-type: none"> <li>FEA of full-scale bridge impacted with a semi-truck trailer</li> <li>Drop-hammer test of PC beam with honeycomb</li> </ul>
2. Steel Girder Protection with Sorbothane <sup>®</sup> High-Impact Rubber	<ul style="list-style-type: none"> <li>(Aly &amp; Hoffmann, 2022)</li> </ul>	<ul style="list-style-type: none"> <li>FEA of simplified semi-truck wind deflector and rigid body truck impacting a steel girder</li> </ul>
3. RC Girder Protection with I-Lam Impact Laminate	<ul style="list-style-type: none"> <li>(Qiao, Yang, &amp; Mosallam, 2004)</li> <li>(Qiao P. , Yang, Mosallam, &amp; Song, 2008)</li> <li>(Cheng &amp; Qiao, 2015)</li> </ul>	<ul style="list-style-type: none"> <li>Test RC beam impacted with a wooden impactor</li> <li>FEA of RC beam tests</li> <li>Installed on concrete bridge Delaware, Ohio by the ODOT in 2006</li> <li>Removed from service due to debonding</li> </ul>
4. Steel Railroad Bridge Protection Using Energy Absorbing Steel Crash Beams	<ul style="list-style-type: none"> <li>(Ozadagli, Moreu, Xu, &amp; Wang, 2020)</li> <li>(Xu, et al., 2022)</li> </ul>	<ul style="list-style-type: none"> <li>Pendulum impact test at 1/5 scale of steel girder</li> </ul>
5. Concrete U-Girder Protection with Stiff Guards Backed with Polyurethane Foam	<ul style="list-style-type: none"> <li>(Sharma, 2007)</li> <li>(Sharma, Hurlebaus, &amp; Gardoni, 2008)</li> </ul>	<ul style="list-style-type: none"> <li>Scaled testing of RC beam with steel ball impactor</li> <li>FEA of RC beam tests</li> </ul>

Finally, Section 4 provides a summary of current impact analysis methods of over-height vehicle impact on bridge girders. There is some guidance in existing standards for static design loading on bridges due to vehicular impact. There are also recent studies that develop analytical models to define loading on bridge

girders from over-height vehicles. Likewise, computational models for the vehicles, cargo, and girders are used to define the loading and evaluate the response of the girder, bridge deck, and proposed protection systems. Section 4 provides a summary of these three methods.

Within the discussions of each proposed protection system is an assessment of inspection and instrumentation considerations. In general, the primary factors influencing inspection and instrumentation methods address how the protection systems are attached to the girders, whether the attachment is at discrete locations or spread along the surface, and the material and construction of the girders to be protected. The goals of the inspections are to evaluate the effectiveness of the protection system. This would be performed by assessing the level of damage experienced by the girder after various levels of impacts. The techniques used to evaluate the girder condition vary with the girder construction; for example, steel girders versus prestressed or reinforced concrete girders, and details associated with cross-sectional shapes such as I-beams or box girders. Protection systems with mechanical connections to the girders would be preferred over adhesive bonding considering inspection and replacement perspectives. Mechanically connected systems would be easier to remove, and adhesives would tend to hinder visual inspection and nondestructive evaluation (NDE) techniques used to assess material condition.

Damage assessment methods for the girders may include advanced NDE techniques to track changes in girder condition and/or load tests to identify changes in structural performance. High-resolution photographs and Impact Echo may be employed on concrete girders to identify density of crack formation. Static or dynamic load tests performed on the girder after various levels of impact can track changes in girder stiffness.

Instrumentation and monitoring goals will vary with the type of protection system. For protection systems that are attached to the girder at discrete locations through mechanical means it may be possible to define the load transfer through the protection system to the girder. The use of load cells and strain gages at connections provides a means to define loading rate and amplitude resulting from the impacts. Whereas it may be difficult to accurately define load transfer with relatively flexible energy absorption systems that are continuously bonded to the girders with adhesive.

In all cases, instrumentation and monitoring goals include measuring applied loads and girder reactions, capturing dynamic responses, and girder damage assessment. Instrumentation to define loads and reactions depend on the protection system and girder geometry. Instrument types and installation methods to quantify girder damage vary with the girder material and construction methods. For example, identifying damage to concrete members requires quantifying crack formation, permanent deformation of reinforcement, and/or ruptured strands. Therefore, embedded sensors are recommended for concrete girders, whereas surface mounted strain gages can be applied to steel members will capture elastic and inelastic deformation.

## 2. Energy Absorbing Systems for Protecting Bridge Girders

### 2.1. PC Girder Protection with CFRP Wrap and Honeycomb Energy Absorber

#### 2.1.1. System Description

(Agrawal, El-Tawil, Cao, & Wong, 2022) performed nonlinear FEA crash simulations and drop hammer testing on potential reinforcing and energy-absorbing structures for prestressed concrete (PC) bridge girders. Both a carbon fiber reinforced polymer (CFRP) wrap, and an aluminum honeycomb energy absorber were evaluated. The CFRP wrap is shown in Figure 1 and subject to impacts with a trailer as shown in the FEA model in Figure 2. The analysis showed that the CFRP wrap was ineffective in protecting girders against over-height impact. The authors concluded that “The main reason is that CFRP wrapping did not sufficiently enhance the lateral capacity of the girder”.

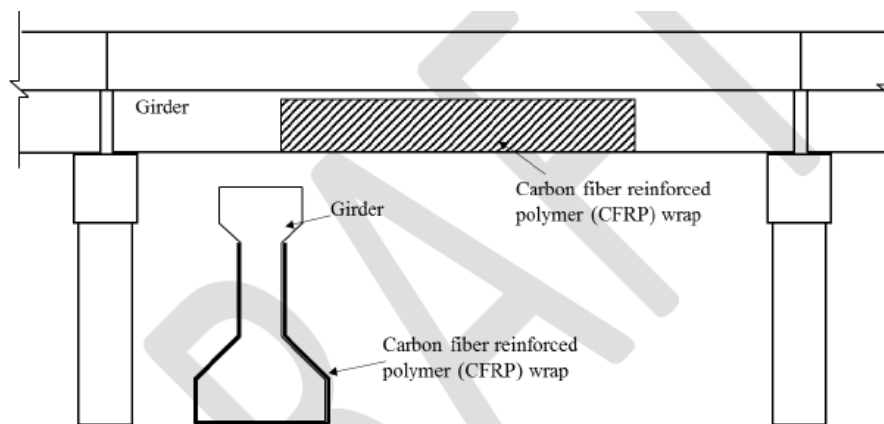


Figure 1. CFRP wrapping of prestressed concrete girders (Agrawal, El-Tawil, Cao, & Wong, 2022).

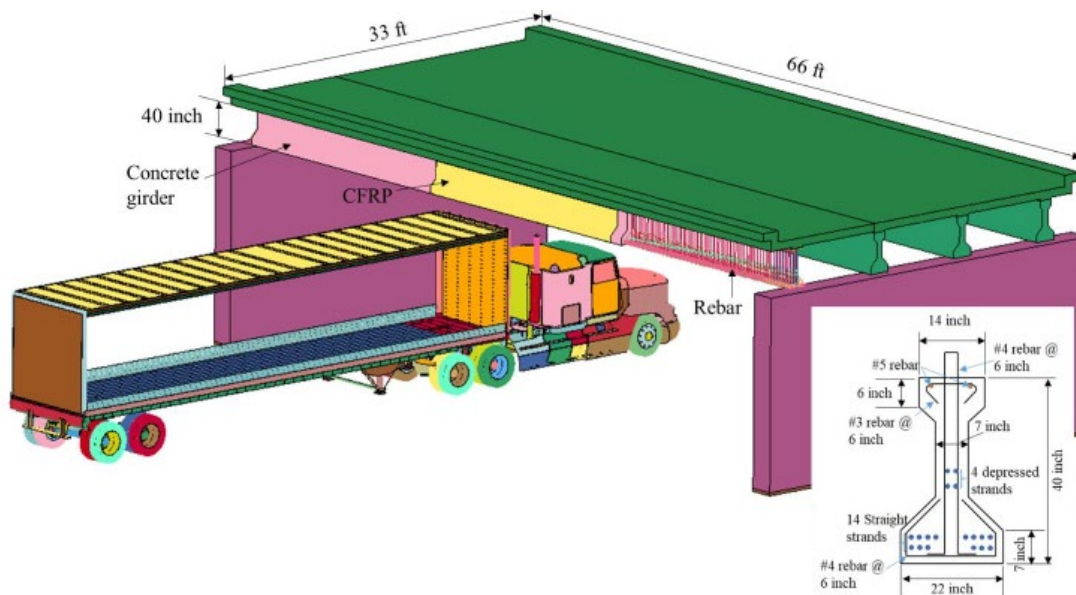
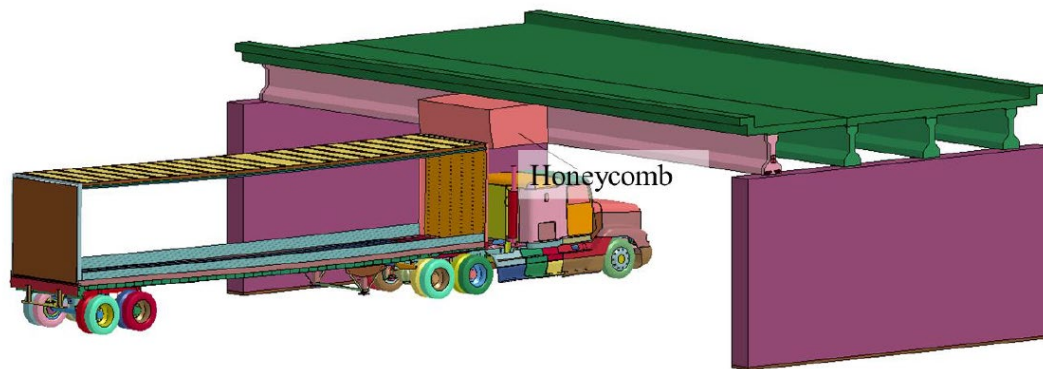


Figure 2. Simulation of a concrete bridge with CFRP wrap on the front girder subject to impact with a trailer (Agrawal, El-Tawil, Cao, & Wong, 2022).

The concept for a honeycomb energy absorber is shown in Figure 3 subject to impacts with a trailer. The honeycomb dimensions are 110 inches x 40 inches (2794 mm x 1016 mm) with a thickness of 80 inches (2032 mm), which was designed to stop the tractor-trailer at a high velocity, up to 113 km/h (70 mph). The analysis showed the honeycomb to be effective in “reducing the impact force transmitted to the protected girders, and they could be designed to dissipate a sufficient amount of energy from the impacting truck so that the girder would be prevented from severe damage and the truck could be stopped” (Agrawal, El-Tawil, Cao, & Wong, 2022).



**Figure 3. Simulation of a concrete bridge with honeycomb attached on the front girder subject to impact with a trailer (Agrawal, El-Tawil, Cao, & Wong, 2022).**

Six tests were carried out on a PC beam with and without honeycomb using a drop hammer, as shown in Figure 4. Honeycomb blocks were attached to the top of the steel beam using epoxy. The honeycomb thickness was 8 inches (203 mm) for the 10-mph (16.1 km/h) impact and 16 inches (406 mm) for the 20-mph (32.2 km/h) impact. Figure 5 shows the deformation of the beam with and without honeycombs, with a reduced deformation when using the honeycomb. The tests displayed reduced strains at the bottom of the beam for cases with honeycomb, as shown in Figure 7 with a reduced permanent strain by 67 percent in the 10-mph (16.1 km/h) case and over 50 percent in the 20-mph (32.2 km/h) case.

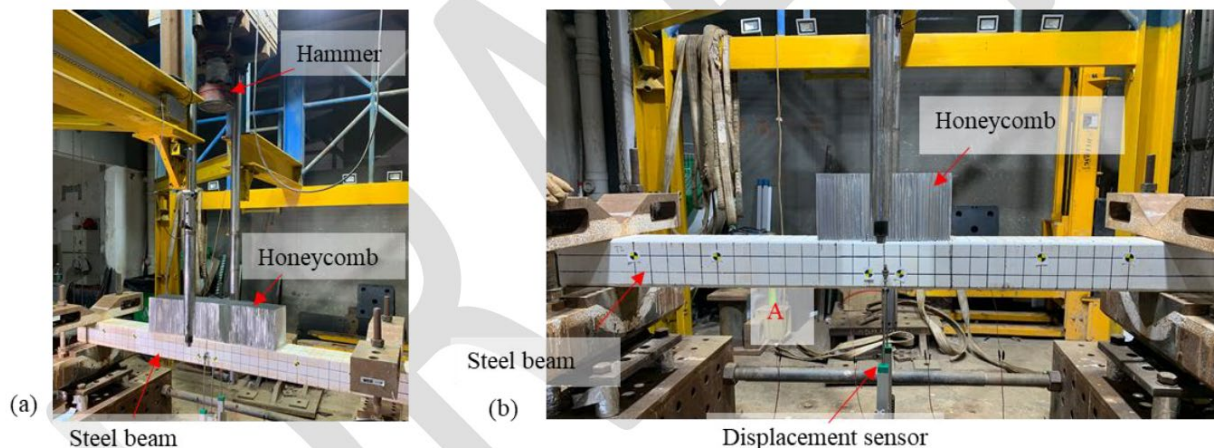


**Figure 4. Drop-hammer test of PC beam with honeycomb (Agrawal, El-Tawil, Cao, & Wong, 2022).**

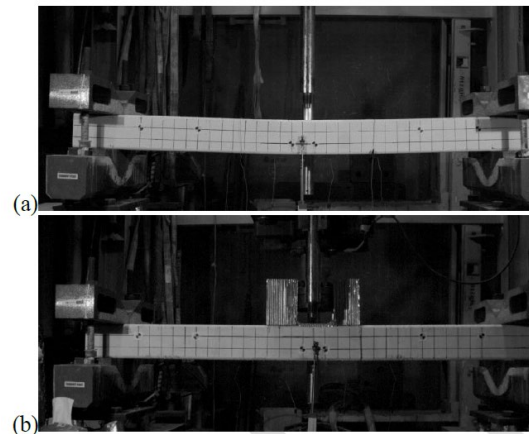


Figure 5. Deformation of the beam from drop-hammer impact at 10 mph with (a) no honeycomb (b) with honeycomb (Agrawal, El-Tawil, Cao, & Wong, 2022).

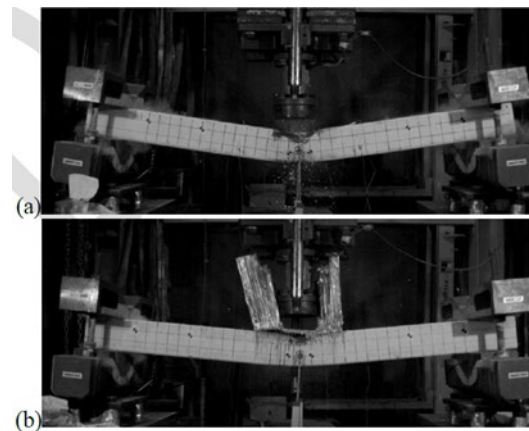


Figure 6. Deformation of the beam from drop-hammer impact at 20 mph with (a) no honeycomb (b) with honeycomb (Agrawal, El-Tawil, Cao, & Wong, 2022).

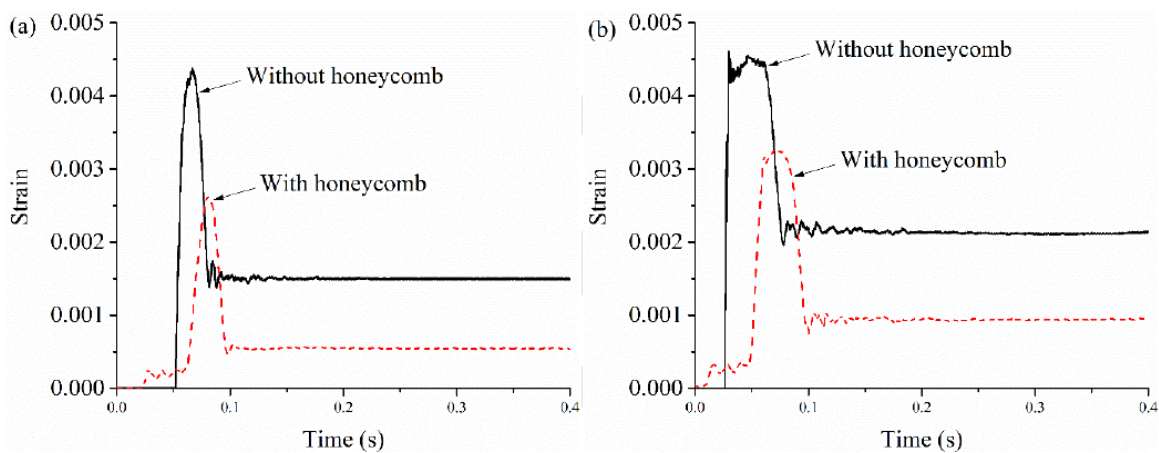


Figure 7. Strain in impact beam from drop-hammer tests (a) at 10 mph and (b) at 20 mph (Agrawal, El-Tawil, Cao, & Wong, 2022).

The authors recommend that a face panel be used to make the honeycomb more effective in protecting the structure. They also recommend combination of CFRP wrap and honeycomb devices so that the capacity of the concrete girder is increased with impact protection from honeycombs, but this approach was not explored.

### 2.1.2. Inspection and Monitoring Considerations

The ability to inspect the bridge girder and determine the effectiveness of the honeycomb devices is dependent on the attachment methods. Ideally, after significant impacts it would be possible to perform a detailed inspection including hands on visual inspection, high-resolution photography, and nondestructive evaluation (NDE) procedures to evaluate concrete crack formations. Ultrasonic Pulse Velocity (UPV) systems provide direct measures of crack depth, while shear wave tomography (MIRA) or other wave speed measurements provide useful relative comparisons of concrete condition after each impact. A thorough inspection of the impacted surface would be difficult if the honeycomb panels were bonded to the concrete with adhesives. Whereas, mechanically fastened panels would simplify removal of the honeycomb panels to facilitate visual and advanced inspection.

Instrumentation goals are to measure girder performance, reactions, and permanent deformation. Direct measurement of load applied to the girder is not practical for this application. Therefore, the influence of the honeycomb absorbers on the applied load signature can only be determined through comparison of girder reactions with and without the bridge bumpers in place. While most instrumentation such as load cells, accelerometers, and displacement sensors can be installed to concrete surfaces to measure deformations, embedded strand meters or instrumented rebar can define internal stress states. The advanced NDE methods of UPV and Ultrasonic Testing (UT) can be used for inspection of concrete members to identify changes in crack density and crack depth. Table 2 provides a list of applicable inspection and monitoring techniques used to evaluate protection performance.

**Table 2. Inspection and Instrumentation Methods – Honeycomb Energy Absorber on PS/C**

Methods	Tools / Sensors	Applicable (Y/N)
Condition Assessment		
Damage assessment	Visual Inspection	Y
Concrete crack formation	High resolution (HR) imaging	Y
Concrete crack formation	NDE (UT, UPV, MIRA)	Y
Permanent deformation	Linear variable differential transducers (LVDT)/Images	Y
Change in girder stiffness	Load Test	Y
Performance Monitoring		
Load Transfer	Load Cells	N
Reactions	Load Cells	Y
Dynamic response displacement	LVDTs / Highspeed Video	Y
Dynamic response	Accelerometers	Y
Dynamic and permanent stress	Strain gages (surface or embedded)	Y

## 2.2. Steel Girder Protection with Sorbothane® High-Impact Rubber

### 2.2.1. System Description

(Aly & Hoffmann, 2022) proposed using a sacrificial cushion system to dissipate the energy of an over-height vehicle impact on steel girders. A material representing a Sorbothane® high-impact rubber was chosen and Ansys Explicit Dynamics models were used to evaluate the proposed designs. The type of girder evaluated is a curved steel plate I-girder attached to a bridge deck as shown in Figure 8. In the analysis, only Girder B was modeled. The floor beams, transverse stiffeners, deck, and Girder A were not modeled. The top flange of the girder is normally cast into the bottom of the deck, so the top flange of the girder in the model was fixed along with the bottom outside edges over a 32-ft (9754 mm) span.

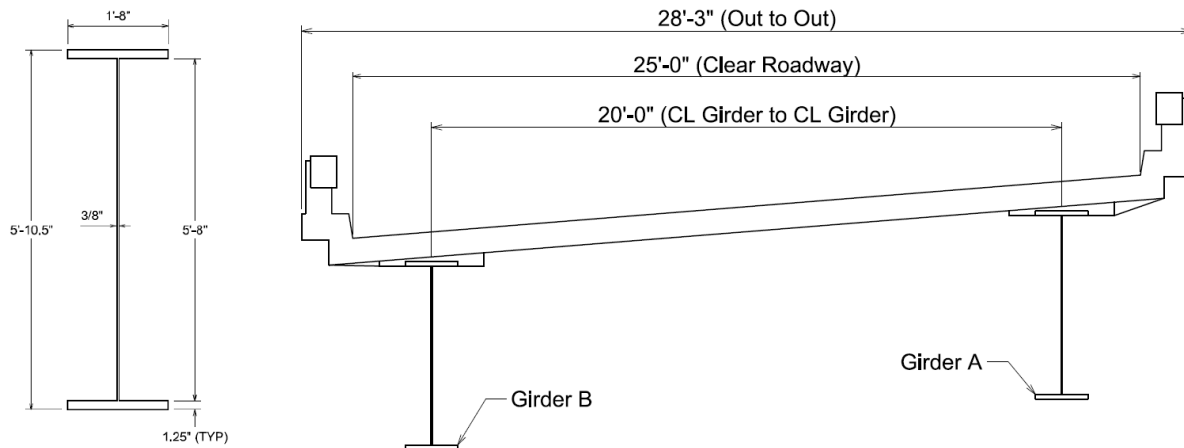


**Figure 8. Bridge and I-girder cross section (Aly & Hoffmann, 2022).**

A semi-truck was chosen as a representative vehicle for the over-height analysis, as shown in Figure 9. The vehicle model was constructed with the wind deflector of the vehicle as deformable and the bottom as a rigid body to provide momentum and rotational stiffness of the vehicle. The top part of the semi-truck that was subjected to the impact force was modeled as a thin-walled deformable element with a steel wall thickness of 0.05 inch (1.3 mm). The box was attached to the vehicle at the bottom four corners. Total vehicle weight is 82,254 pounds (37,310 kg). The height of impact above the bottom flange of the girder is 7 inches (178 mm) and the vehicle model was initialized at 70 mph (113 km/h).



**Figure 9. Over-height vehicle selected for analysis (Aly & Hoffmann, 2022).**

Two configurations using the Sorbothane® high-impact rubber were analyzed. The first is a cushion of rubber positioned to extend 3 inches past the bottom flange of the girder to shield the bottom flange from impact. The second is a sandwich structure with the rubber between two stiff plates. The outside stiff plate acts as the first point of contact with the vehicle and transfers the load to the Sorbothane®, which dampens

forces of impact. The sandwich system extends for a total of 1.0 ft (305 mm) in front of the bottom flange of the girder. No explanation was provided for potential attachment schemes.

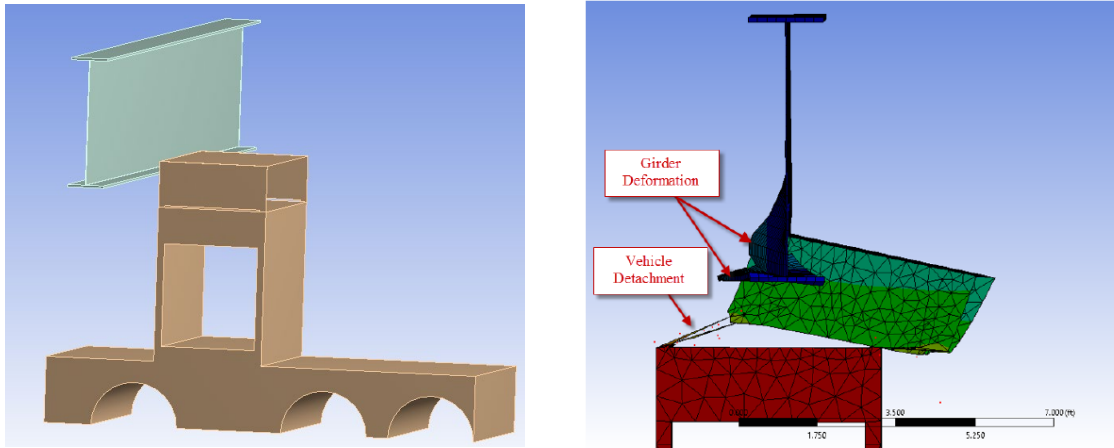
The final model configurations and results from the analyses of each configuration are shown in Figure 10. The baseline response of the girder impacted with the truck is shown in Figure 10(a). Both protection schemes reduce the lateral deflection of the girder bottom flange. The rubber cushion alone reduced the deformation in the bottom flange by roughly 23 percent laterally and 8 percent vertically from that of the unprotected girder. The sandwich system exhibited the best results reducing the lateral deflection in the bottom flange by 91% and the vertical by 95%.

### 2.2.2. Inspection and Monitoring Considerations

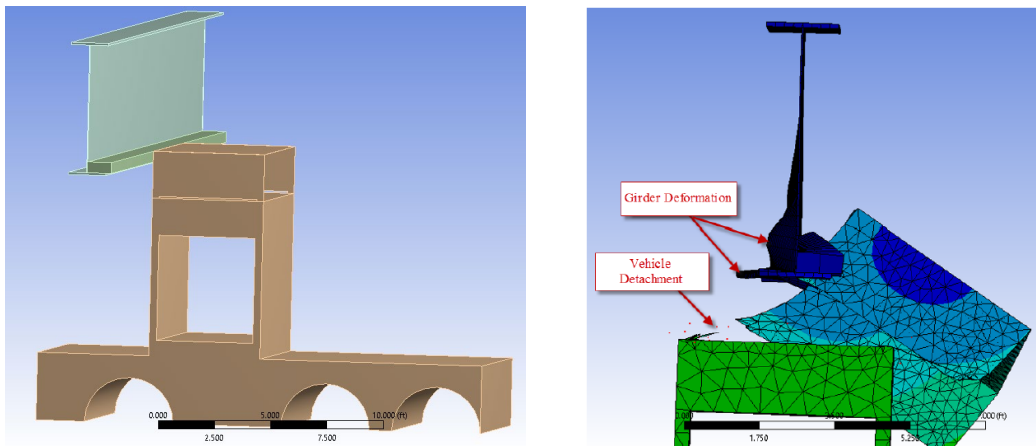
Inspection and instrumentation goals on steel girders will be to determine dynamic performance and measure permanent deformations. Direct application of Sorbothane® would likely have a distributed bearing between the steel such that direct measurement of load transfer is not feasible. Therefore, the influence of the Sorbothane® on the load signature applied to the girder would likely be determined from comparison of girder reactions with and without the protection in place. The measurement focus would be on the stress, displacement, and reactions of the steel girder. Effectiveness would be determined by measured stress levels and girder damage in the form of yielding and/or fracture of the steel. Table 3 provides a list of applicable inspection and monitoring techniques used to evaluate protection performance.

**Table 3. Inspection and Instrumentation Methods – Sorbothane® on Steel**

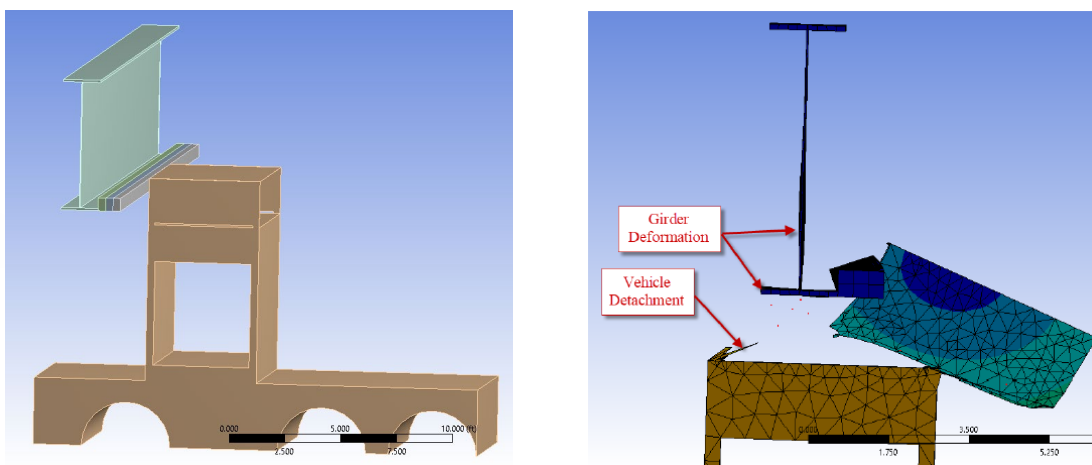
Methods	Tools / Sensors	Applicable (Y/N)
Condition Assessment		
Damage assessment	Visual Inspection	Y
Concrete crack formation	HR imaging	N
Concrete crack formation	NDE	N
Permanent deformation	LVDTs / Images	Y
Change in girder stiffness	Load Test	N
Performance Monitoring		
Load Transfer	Load Cells:	
	Sorbothane® only	N
	Sorbothane® w/steel plates	Y
Reactions	Load Cells	Y
Dynamic response displacement	LVDTs / Highspeed Video	Y
Dynamic response	Accelerometers	Y
Dynamic and permanent stress	Strain gages (surface or embedded)	Y



(a) Impact with the steel girder



(b) Impact with Sorbothane<sup>®</sup> high-impact rubber cushion



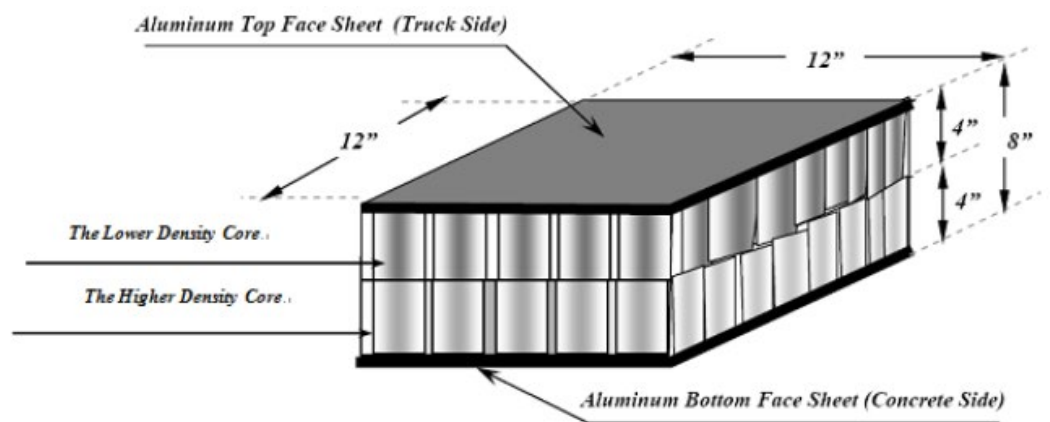
(c) Impact with Sorbothane<sup>®</sup> high-impact rubber sandwich structure

**Figure 10. Vehicle-girder impact Ansys analysis 70 mph (113 km/h) (Aly & Hoffmann, 2022).**

## 2.3. RC Girder Protection with I-Lam Impact Laminate

### 2.3.1. Systems Description

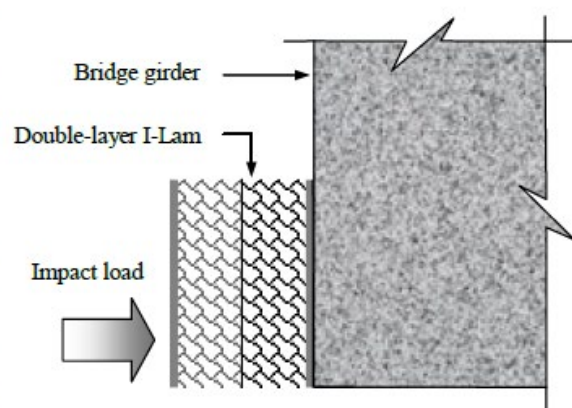
An aluminum honeycomb impact laminate called ‘I-Lam’ shown in Figure 11 was developed by several authors to protect reinforced concrete (RC) bridge girders (Qiao, Yang, & Mosallam, 2004), (Qiao P. , Yang, Mosallam, & Song, 2008), (Cheng & Qiao, 2015). The I-Lam configuration has two different density honeycomb layers [90-psi (621 kPa) front layer and 210-psi (1448 kPa) rear layer] with a front and back aluminum face sheet. The density honeycomb is designed for the impact/collision of lighter over-height materials and low speed; while the higher density honeycomb is intended for the case of heavier over-height sheared-off materials and high speed. Explicit finite element analysis (FEA), analytical modeling, and component testing were used to design this system that was ultimately installed on bridge DEL-23-12.99 in Delaware, OH on Nov. 1, 2006. The installation is shown in Figure 12. Details on installation are provided in Section 2.3.2.



(a) I-Lam configuration



(b) An actual I-Lam panel



(c) Schematic of I-Lam in application

**Figure 11. Double-layer I-Lam sandwich system for collision protection (Cheng & Qiao, 2015).**



**Figure 12. Final installed I-Lam panel on bridge DEL-23-12.99 (Qiao P. , Yang, Mosallam, & Song, 2008).**

Full-scale impact tests were performed by (Qiao P. , Yang, Mosallam, & Song, 2008) on a RC beam shown in Figure 13 to evaluate the level of protection from the I-Lam. Tests were performed with and without the I-Lam using a 12 x 12 x 12-inch (305 x 305 x 305-mm) wooden projectile at an impact speed of 45 mph (72 km/h). Load cells installed at the supports of the RC beams were used to measure reaction forces. The experimental setup is shown in Figure 14.

(Cheng & Qiao, 2015) also performed FEA simulations of the full-scale impact tests and compared the results with experimental data and observations. Simulated crushing of the I-Lam after a test is compared with the FE simulation in Figure 15. Simulated tensile damage to the RC beam with and without the I-Lam is shown in Figure 16. The tensile damage in the unprotected beam is much more severe. Likewise, the peak reaction forces are reduced by about 42 percent, as shown in Table 4.

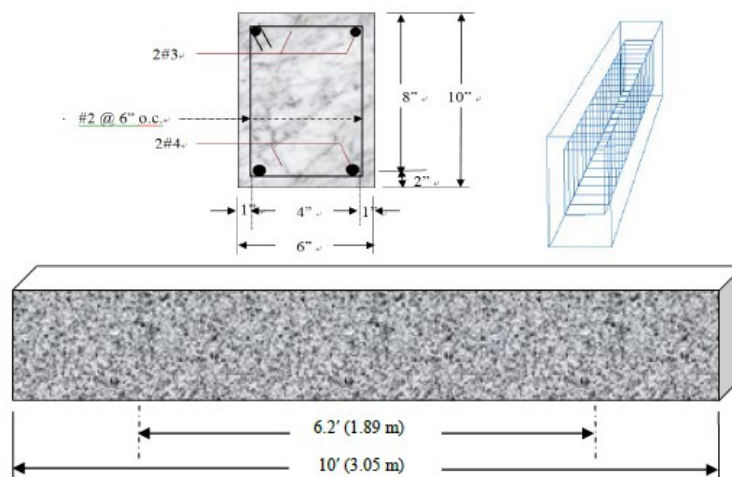
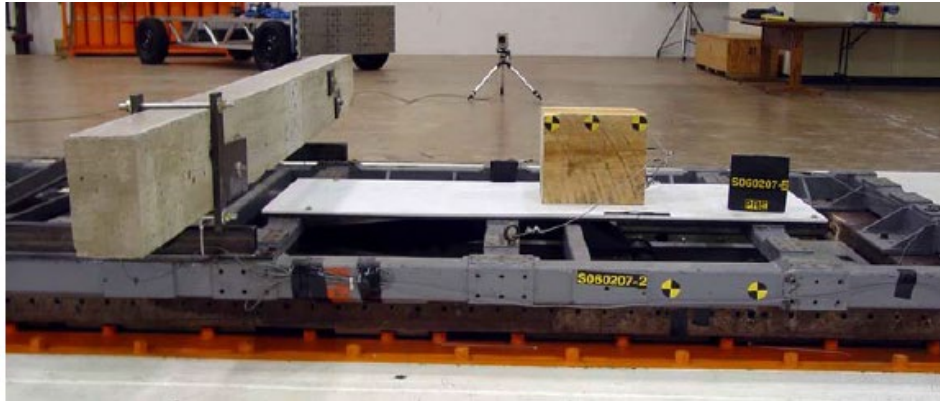
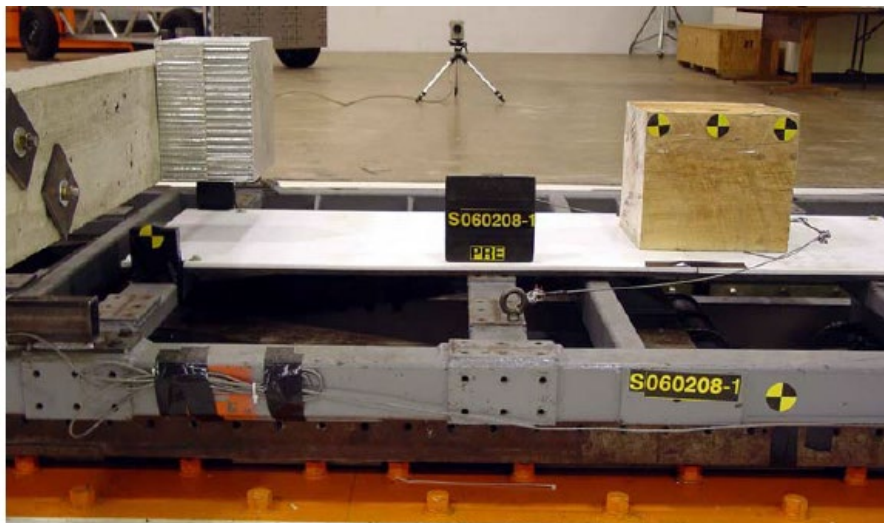


**Figure 13. Geometry of the RC beam used in impact testing of the I-Lam (Cheng & Qiao, 2015).**

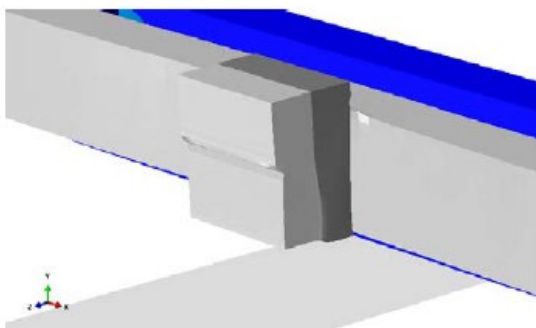


(a) Without I-Lam



(b) With I-Lam

*Figure 14. Impact test set-up of the RC beam impacted with a wooden impactor (Qiao P., Yang, Mosallam, & Song, 2008).*



(a) FE simulation



(b) Experimental phenomenon

*Figure 15. I-Lam panel after impact (Cheng & Qiao, 2015).*

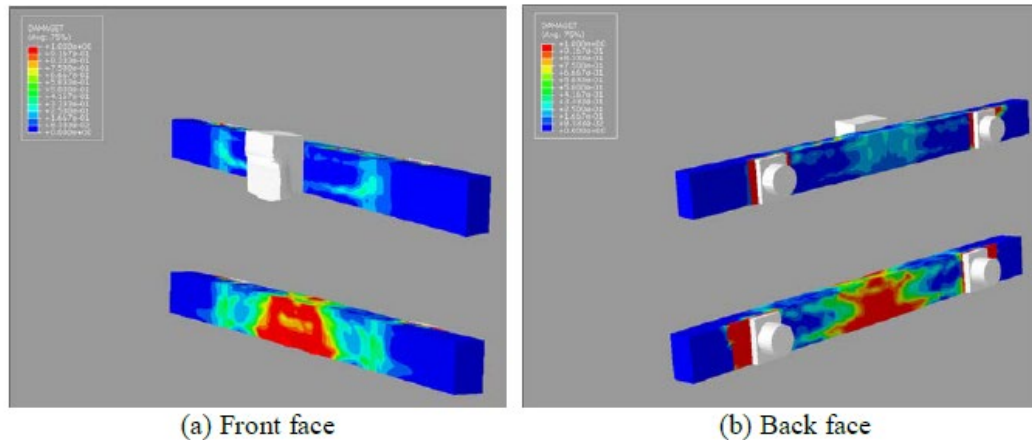


Figure 16. Tensile damage of the RC after impact (Cheng & Qiao, 2015).

Table 4. Comparisons of the maximum reaction forces due to impact (Cheng & Qiao, 2015)

Samples	Time (s)		Maximum reaction force (kN)	
	Test	FE	Test	FE
Bare RC beam	0.096	0.097	65.4	58.6
I-Lam protected RC beam	0.0967	0.0963	38.2	39.5

### 2.3.2. Installation and Performance on ODOT Bridge

Installation and attachments of the I-Lam is described in (Qiao P. , Yang, Mosallam, & Song, 2008), as shown in Figure 17. The authors propose that the I-Lam panels can be either adhesively bonded or bolted to the concrete girders. Two cables are attached to each I-Lam panel and the RC to keep individual I-Lam from falling on traffic below. Multiple I-Lam panels are meant to be installed along the length of a girder with 1-inch clearance between units, as shown in Figure 18. As was shown in Figure 12, the I-Lam panels were installed on a slab concrete bridge (DEL-23-12.99) in Delaware, Ohio by the ODOT District 6 on Oct. 31 to Nov. 1, 2006. A total of 20 I-Lam panels were installed over an installed length of about 20 ft (6096 mm). This installation resulted in some of the units falling off over time due to debonding. The system was finally removed due to the risk of falling on traffic (Abu-Hajar, 2024). No information was available on the cause of debonding, but environmental issues may have been an issue. It was not struck by any vehicles prior to being removed.

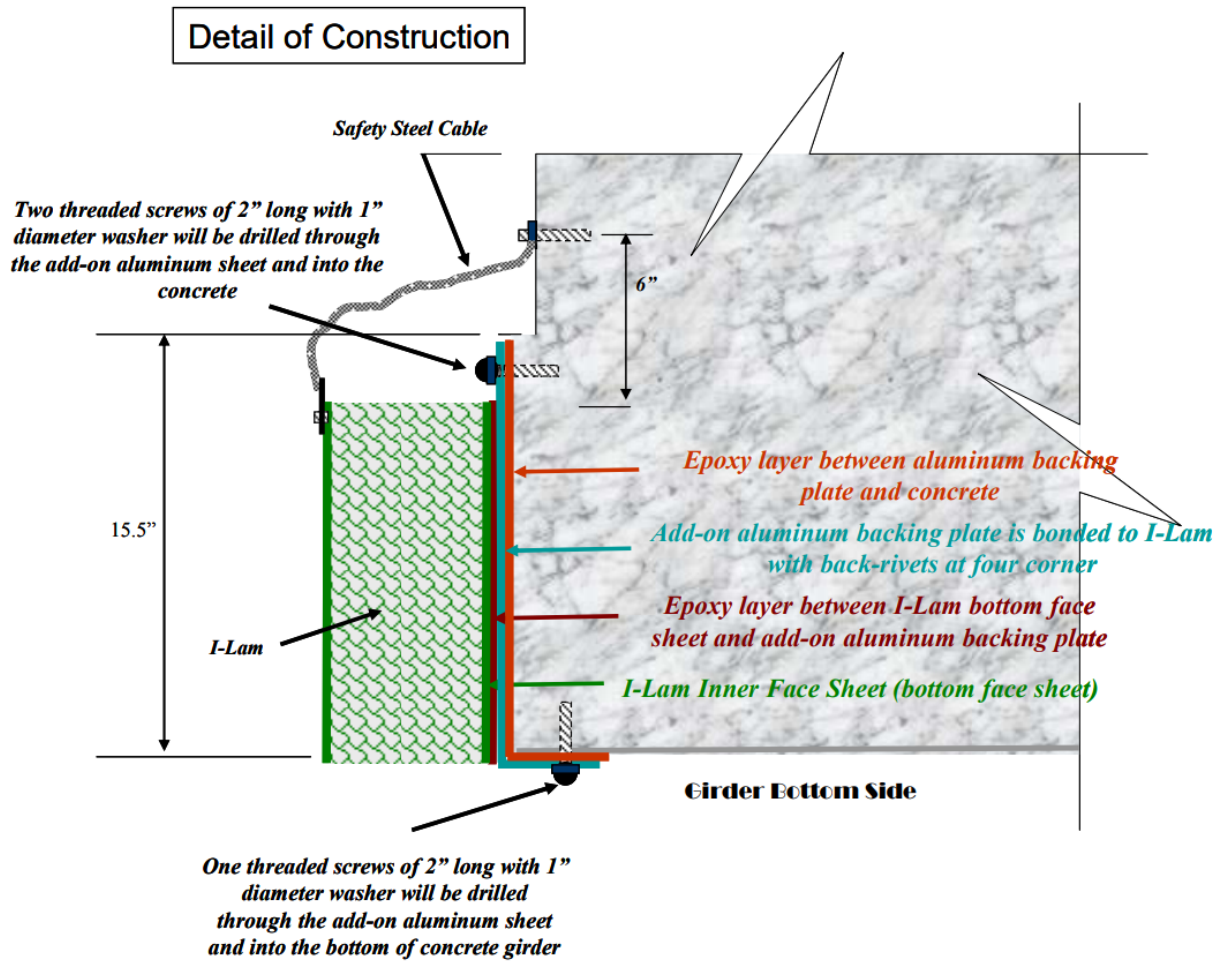
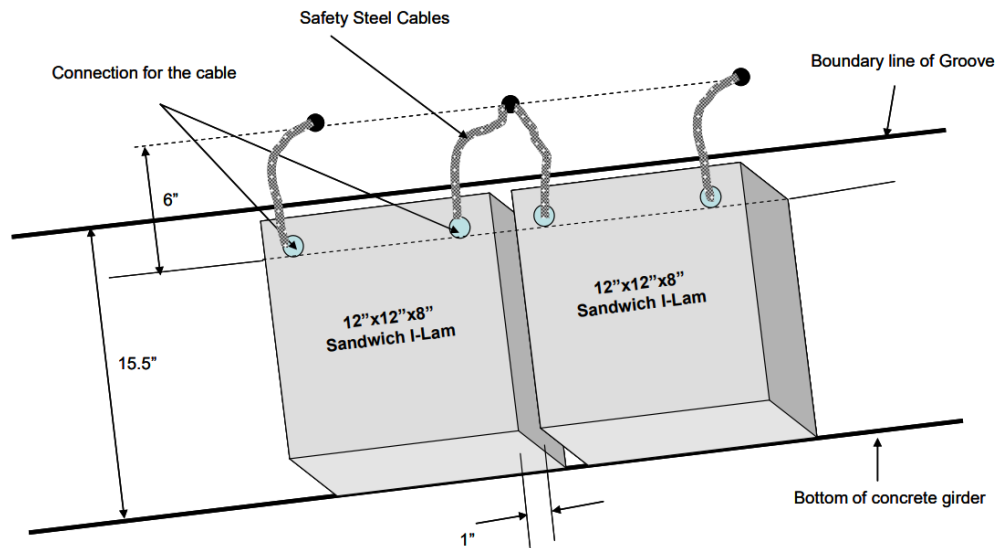


Figure 17. Details of the original I-Lam installation (Qiao P. , Yang, Mosallam, & Song, 2008).



**Figure 18. Schematic of I-Lam installed along the bottom of a RC girder (Qiao P. , Yang, Mosallam, & Song, 2008).**

### 2.3.3. Inspection and Monitoring Considerations

Inspection and instrumentation considerations are essentially identical to the Honeycomb protection system. The goal is to assess the applied loads and the concrete member condition along with evaluating changes in performance after various levels of impact. Condition assessment would be performed through a detailed inspection including hands on visual inspection, high-resolution photography, and NDE procedures to evaluate concrete crack formations. A mechanically fastened protection system would be preferred over adhesive bonding to facilitate inspection and NDE investigations.

Instrumentation goals would include applied load, girder performance measures, reactions, and permanent deformation. While most instrumentation such as load cells, accelerometers, and displacement sensors would be installed to concrete surface, embedded instrumented rebar would be beneficial to determine change in girder stress state. Influence of the I-Lam system on the load signature applied to the girder would likely be determined from comparison visual inspection and from the girder reactions with and without the bridge bumpers in place. Table 5 provides a list of applicable inspection and monitoring techniques used to evaluate protection performance.

**Table 5. Inspection and Instrumentation Methods – I-Lam Impact Laminate**

Methods	Tools / Sensors	Applicable (Y/N)
Condition Assessment		
Damage assessment	Visual Inspection	Y
Concrete crack formation	HR imaging	Y
Concrete crack formation	NDE	Y
Permanent deformation	LVDTs / Images	Y
Change in girder stiffness	Load Test	Y
Performance Monitoring		
Load Transfer	Load Cells	N
Reactions	Load Cells	Y
Dynamic response displacement	LVDTs / Highspeed Video	Y
Dynamic response	Accelerometers	Y
Dynamic and permanent stress	Strain gages (surface or embedded)	Y

## 2.4. Steel Railroad Bridge Protection Using Energy Absorbing Steel Crash Beams

### 2.4.1. System Description

(Ozadagli, Moreu, Xu, & Wang, 2020) and (Xu, et al., 2022) performed scaled model testing of energy absorbing steel crash beams to protect ballast deck through plate girder (TPG) steel bridges from over-height vehicle impact. A typical example of a ballast deck TPG steel bridge is shown in Figure 19. The authors selected TPG bridges because the railroads indicated that type is hit most frequently. A schematic showing one of the steel crash beams evaluated attached to the TPG bridge is shown in Figure 20. The beam spans 15.25 m (50 ft) and is attached with C-channel supports. Four types of crash beams were evaluated as shown in Figure 21. Crash beam Type 1 consists of one steel plate connected to the bridge at six locations. Types 2, 3 and 4 use an I-beam at the impact faces and are connected at 3, 6, and 11 locations, respectively. All are made of Q235 steel. All are fastened to the girder using the bolted connection shown in Figure 22. Energy absorption occurs through the plastic deformation of the impact beam and the C-channels.

Impact testing was performed using scaled test articles at 1:5 using similitude per the Buckingham  $\pi$ -theorem. The pendulum test frame is shown in Figure 23 along with the scaled test articles attached to the girder. Experiments were run with and without the various crash beam designs at impact energy levels categorized as ‘low’, ‘medium/intermediate’ and ‘high/severe’ that were achieved by changing impact speed with the height of the pendulum. Test configurations are shown in Figure 24.



Figure 19. Typical through plate girder railroad bridge over a highway overpass (Xu, et al., 2022).

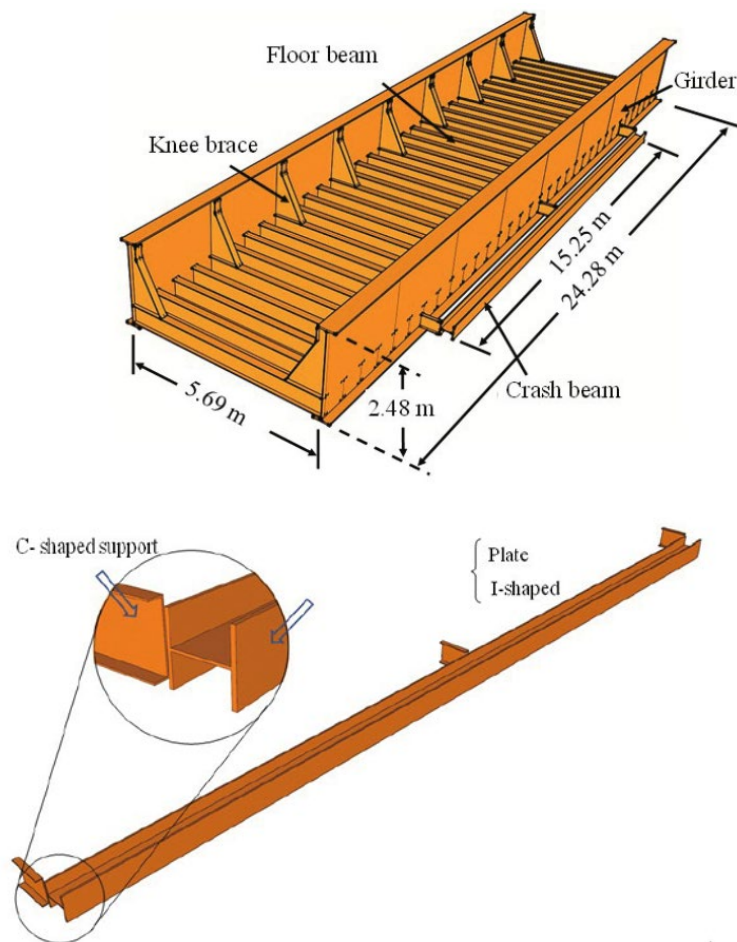


Figure 20. Schematic of (a) TPG steel bridge with a crash beam attached and (b) attachment details (Xu, et al., 2022).

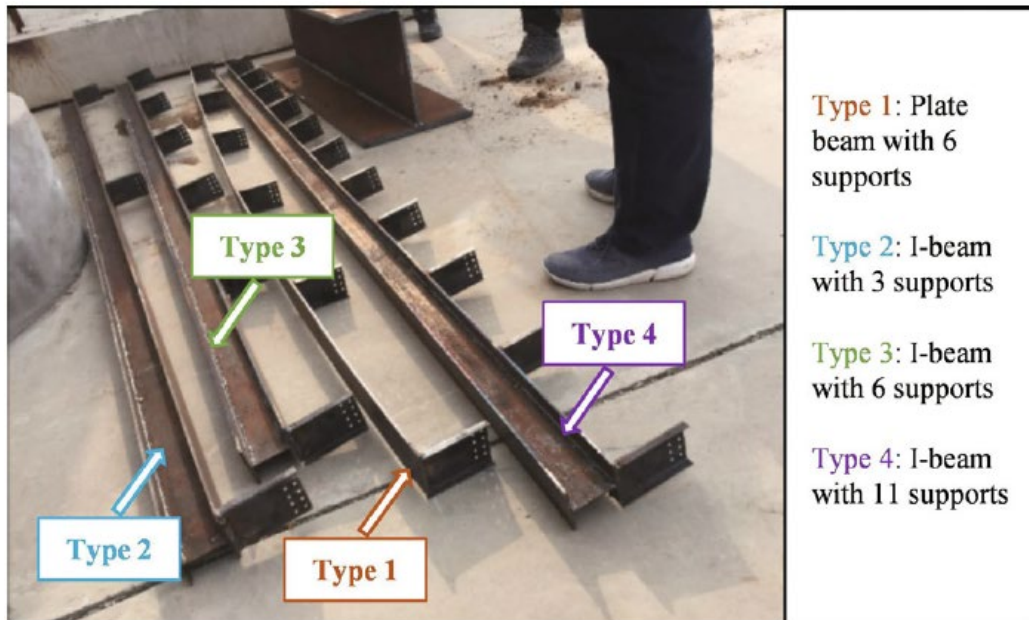


Figure 21. Crash beam test articles (Xu, et al., 2022).

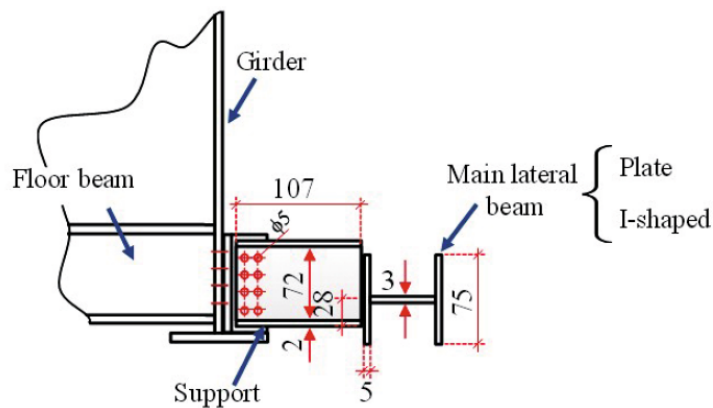
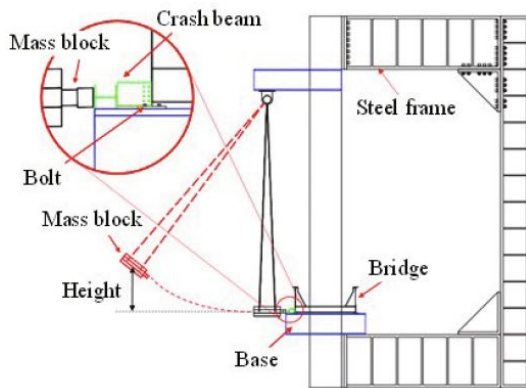


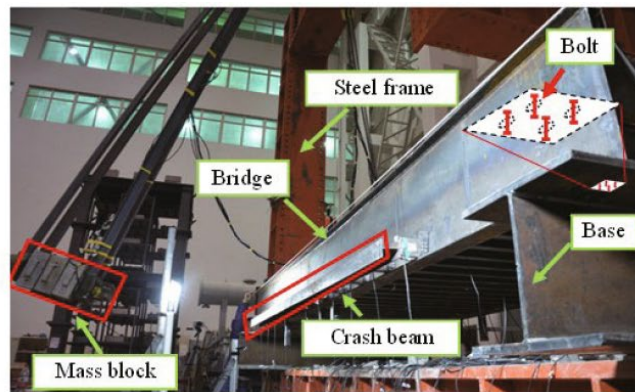
Figure 22. Installation details for the crash beams using bolted C-channel supports (mm) (Xu, et al., 2022).



(a)



(b)



(c)

**Figure 23. Testing frame (a) loading frame with scaled girder (Ozadagli, Moreu, Xu, & Wang, 2020) (b) test frame schematic (c) complete test setup with impact block (Xu, et al., 2022).**

<p style="text-align: center;">No-Crash Beam</p>	<p style="text-align: center;">Plate + 6 Connection</p>
<p style="text-align: center;">I-Beam + 3 Connection</p>	<p style="text-align: center;">I-Beam + 6 Connection</p>

**Figure 24. Crash beam configurations (Ozadagli, Moreu, Xu, & Wang, 2020).**

The authors evaluated the performance of each crash beam design relative to test results with no beam using an attenuation calculated from the LVDT measurement locations (D1, D2, and D3) shown in Figure 25. The attenuation was calculated as

$$Attenuation = \frac{\Delta_{crash\ beam} - \Delta_{no-crash\ beam}}{\Delta_{no-crash\ beam}} \quad (1)$$

where  $\Delta_{crash\ beam}$  is the maximum total displacement of the outside (impacted) girder of the bridge when a crash beam is attached and  $\Delta_{no-crash\ beam}$  is the displacement of the bridge girder in the absence of a crash beam.

Attenuation results are shown in Table 6 and Table 7. In Table 6, only the largest displacement from the three measurement locations is used to calculate attenuation at each intensity level for Type 1 (plate + 6 connections), Type 2 (I-beam + 3 supports) and Type 3 (I-beam + supports). Cases where the crash beam was severely damaged were denoted as ‘Failure’. For low impact energy levels, Type 1 and Type 2 beams attenuate similarly. At intermediate intensity, Type 2 (with less connections) attenuates better than Type 3.

**Table 6. Attenuation (%) of total bridge girder displacements (Ozadagli, Moreu, Xu, & Wang, 2020)**

Type	Impact intensity (increases from left to right)		
	Low intensity	Intermediate intensity	High intensity
Plate + 6 connection	21.0	Failure	Failure
I-beam + 3 connection	23.0	45.5	Failure
I-beam + 6 connection	N/A	34.7	24.0

The better attenuation performance of the plate beam over the I-beam at low-intensity and the I-beam with three connections over six connections at intermediate-intensity suggests that weaker beams impose better energy absorption and less energy transmission to the bridge superstructure. However, there is also a tradeoff between the beam’s energy absorption capability and its force resistance capacity (e.g., an I-beam with six connections can resist larger impact loads, whereas an I-beam with three connections and a plate beam fail). Finally, an I-beam with six connections attenuates displacements up to 52%.

Table 7 provides further detail on the attenuation at each measurement location for the intermediate/moderate and high/severe impact intensities and includes the Type 4 crash beam (with 11 connections). The authors point out that under moderate impact conditions the beam configurations with more support have less attenuation. The average attenuation decreased from 83.4% to 43.39% when the number of supports increased from 3 to 11. For severe impacts the Type 4 crash beam attenuated deformation by 43.03%. The results demonstrate that all the proposed crash beams were effective in attenuating residual deformation of the scaled bridge girder for varied categories of impact energy. The authors recommend balancing the lateral beam stiffness and the number of supports and their stiffness in the design of the optimal crash beam against lateral impact.

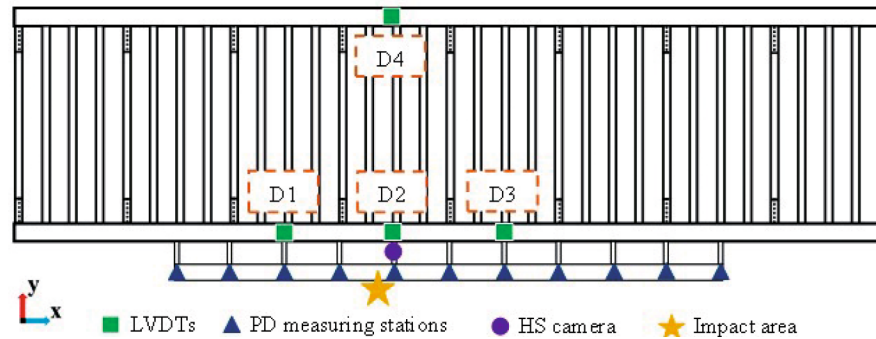


Figure 25. Test instrumentation (Xu, et al., 2022).

Table 7. Residual deformation and attenuation (%) of bridge girder displacements (Xu, et al., 2022)

	Station	Moderate impact (20 - 30 kN)				Severe impact ( $\geq 30$ kN)	
		Design force: 30 kN				Design force: 50 kN	
		Type 2	Type 3	Type 4	No beam	Type 4	No beam
Residual deformation (mm)	D1	0.7	0.76	3.2	5.71	10.75	19.93
	D2	0.62	0.28	2.29	6.09	12.37	24.47
	D3	0.62	0.69	1.97	3.09	13.1	20.82
	D4	0.71	0.88	2.05	2.97	13.31	22.01
Attenuation (%) $= \frac{d_{\text{no beam}} - d_{\text{crash beam}}}{d_{\text{no beam}}} \times 100\%$	D1	87.74	86.69	43.96	--	46.06	--
	D2	89.82	95.40	62.40	--	49.45	--
	D3	79.94	77.67	36.25	--	37.08	--
	D4	76.09	70.37	30.98	--	39.53	--
Average (%)	--	83.40	82.53	43.39	--	43.03	--

#### 2.4.2. Inspection and Monitoring Considerations

The steel crash beam system has several advantages from an inspection and monitoring perspective primarily because the system and the girder are both steel. With everything being exposed, it would be easy to examine the condition and permanent deformations of the crash beam and the exterior girder since there are no adhesive coatings or CFRP wraps to inhibit visual inspection. With regards to instrumentation, the connections between the crash beam and exterior girder provide opportunities to include load cells or strain gages so that loads applied to the girder could be measured directly. Applied loading rate, load magnitudes, and load paths through the system would provide highly valuable research data.

As with all the protection systems, monitoring of dynamic girder responses, girder reactions, and permanent deformations could readily be performed. Strain gage applications on steel systems tend to be easier, less expensive, and have better accuracy compared to strain measurements within concrete components. Table 8 provides a list of applicable inspection and monitoring techniques used to evaluate protection performance.

**Table 8. Inspection and Instrumentation Methods – Steel Crash Beam**

Methods	Tools / Sensors	Applicable (Y/N)
Condition Assessment		
Damage assessment	Visual Inspection	Y
Concrete crack formation	HR imaging	N
Concrete crack formation	NDE	N
Permanent deformation	LVDTs / Images	Y
Change in girder stiffness	Load Test	N
Performance Monitoring		
Load Transfer	Load Cells or strain gages	Y
Reactions	Load Cells	Y
Dynamic response displacement	LVDTs / Highspeed Video	Y
Dynamic response	Accelerometers	Y
Dynamic and permanent stress	Strain gages (surface or embedded)	Y

## 2.5. Concrete Box-Girder Protection with Stiff Guards Backed with Polyurethane Foam

### 2.5.1. System Description

(Sharma, 2007) and (Sharma, Hurlebaus, & Gardoni, 2008) proposed a bridge bumper consisting of a stiff guard backed by high-density flexible polyurethane foam to protect concrete box-girders as shown in Figure 26. The ‘stiff guard’ distributes concentrated impacts from an over-height vehicle over a larger area, decreasing stresses at the point of impact. The foam absorbs energy during impact. The authors performed impact experiments on a RC beam with and without the ‘bridge bumper’ and used acceleration data from these tests to validate a FE model of the test. The FE results were then used to evaluate performance. No consideration was given for a connection scheme, to determine vehicle interaction with the bumper, or predict damage to a bridge. The authors did provide first-order methods for scaling test results to a full-scale application.

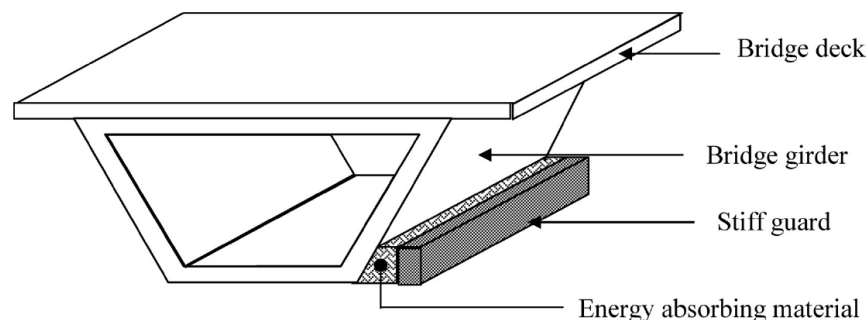


**Figure 26. Sketch of bridge bumper to protect a box-girder (Sharma, Hurlebaus, & Gardoni, 2008).**

A set of small-scale experiments were performed by the authors consisting of a RC beam, a layer of energy-absorbing material (EAM) and a stiff guard on the impact face, as shown in Figure 27. Each layer of the bridge bumper was attached to the adjacent layer using double-sided tape. The beam is meant to represent a scaled model of a bridge girder. It is 1.04 m long, with a cross section of 105×103mm (4.13×4.06

inches), and two No. 4 bars spaced 20 mm (0.79 inches) from the bottom face. The stiff guard is 3.175 mm (0.125 inches) thick steel plate with a dimensions of 1.04 m x 0.105 m (40.9 x 4.13 inches). All tests were performed at a fixed impactor height with an impact speed of 5.9 m/s (13.2 mph). The impactor is a steel ball of varied weights [67 g, 228 g, 540 g (0.15 lb, 0.503 lb, 1.19 lb)]. Four types of high-density flexible polyurethane foam were evaluated as EAM. Each was tested at 50 mm thick. The stress-strain response of each foam is shown in Figure 28. Each foam type displays 51 percent hysteresis upon unloading.

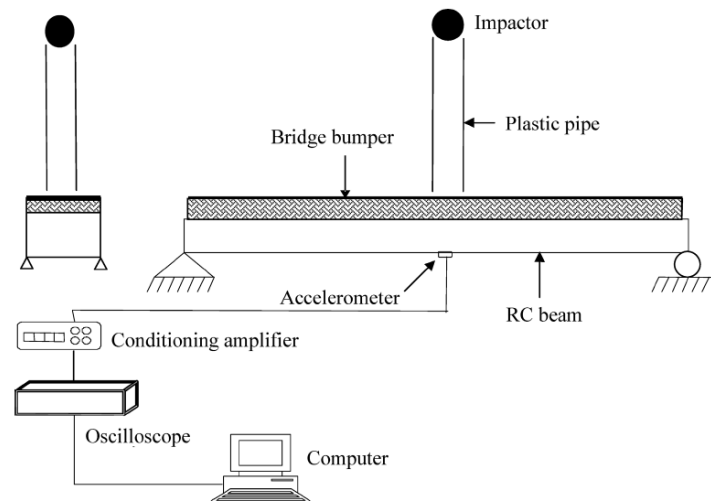


**Figure 27. Experimental setup for impact testing of the bridge bumper (Sharma, Hurlebaus, & Gardoni, 2008).**

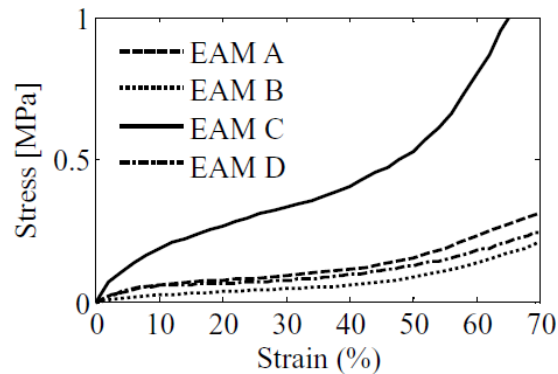


**Figure 28. Stress-strain for four EAM tested (Sharma, Hurlebaus, & Gardoni, 2008).**

The authors then performed an LS-DYNA FE simulation of the test and demonstrated good agreement between the measured accelerations and the simulation results. Values for the peak tensile and compressive stress in the RC beam, the peak acceleration and others derived from the FE simulation are shown in Table 9. These results demonstrate that the proposed bridge bumper significantly reduces the acceleration, stresses and impact force for the impactor selected. Tensile and compressive stresses, which would lead to eventual fracture of the beam, are reduced the most with the least stiff material (EAM B) but may have the least capacity to mitigate higher energy impacts. The authors then perform a numerical optimization to determine a material behavior that would provide optimal performance for this impactor. They identified nitrile rubber and urethane rubber as potential candidates.

**Table 9. Simulated Performance of the Bridge Bumper Using Different EAM with the 67g Impactor (Sharma, Hurlebaus, & Gardoni, 2008).**

<i>Configuration</i>	<i>Tensile stress [MPa]</i>	<i>Compressive stress [MPa]</i>	<i>Energy absorbed by EAM [Nm]</i>	<i>Contact force of beam [kN]</i>	<i>Abs. max. acceleration [m/s<sup>2</sup>]</i>	<i>Abs. min. acceleration [m/s<sup>2</sup>]</i>
Beam without bridge bumper	1.76	17.0	0.00	7.77	151.3	160.9
Beam with stiff guard	1.64 (-7%)	8.57 (-50%)	0.00	13.9 (79%)	127.5 (-16%)	118.0 (-26%)
Bridge bumper with EAM A	0.58 (-67%)	0.66 (-96%)	0.32 (27.9%)	0.49 (-94%)	26.4 (-82%)	24.5 (-85%)
Bridge bumper with EAM B	0.47 (-73%)	0.43 (-98%)	0.24 (20.9%)	0.31 (-96%)	21.5 (-85%)	22.5 (-86%)
Bridge bumper with EAM C	1.41 (-20%)	1.36 (-92%)	0.50 (43.5%)	0.92 (-88%)	41.7 (-72%)	42.6 (-74%)
Bridge bumper with EAM D	0.65 (-63%)	0.56 (-97%)	0.42 (36.6%)	0.47 (-94%)	32.1 (-78%)	37.8 (-77%)

### 2.5.2. Inspection and Monitoring Considerations

From an inspection and monitoring perspective, this system has similar issues as the other flexible energy absorbing systems that are connected to the girders in a uniform fashion. Direct measurement of load applied to the girders would be difficult since the load is not transferred at discrete points. Therefore, instrumentation would be focused on monitoring of dynamic girder responses, girder reactions, and permanent deformations. Influence of the EAM on the load signature applied to the girder would likely be determined from comparison of girder reactions with and without the bridge bumpers in place.

Visual inspection would focus on the level of damage induced on the concrete girder and permanent deformations within the bumper itself. Use of mechanical connections would be beneficial to facilitate the ability to perform inspection and condition assessment of the concrete girder. Examination of crack density, size and depth would be hindered by systems attached with adhesives.

Effectiveness of the protection system would be determined by examining the level of damage experienced by the girder after various levels of impact. Damage evaluation would include visual inspection along with various NDE techniques including impact echo, ultrasonic pulse velocity, and HR imaging. In addition, controlled diagnostic load tests could be performed to evaluate change in girder stiffness. Table 10 provides a list of applicable inspection and monitoring techniques used to evaluate protection performance.

*Table 10. Inspection and Instrumentation Methods*

<b>Methods</b>	<b>Tools / Sensors</b>	<b>Applicable (Y/N)</b>
<b>Condition Assessment</b>		
Damage assessment	Visual Inspection	Y
Concrete crack formation	HR imaging	Y
Concrete crack formation	NDE	Y
Permanent deformation	LVDTs / Images	Y
Change in girder stiffness	Load Test	Y
<b>Performance Monitoring</b>		
Load Transfer	Load Cells or strain gages.	N
	Pressure Sensitive Film	Y
Reactions	Load Cells	Y
Dynamic response displacement	LVDTs / Highspeed Video	Y
Dynamic response	Accelerometers	Y
Dynamic and permanent stress	Strain gages (surface or embedded)	Y

### 3. Other Protection Methods

A common method for protecting bridges from over-height vehicle impacts on bridge girders is to install a protection beam in front of a bridge. An example of a box beam protection girder installed on bridge is shown in Figure 29. The Bridge Strike Prevention Group (BSPG) in the UK supported the provision of using protection beams. There is an existing standard (Highways England, 2020) that provides guidance. This protection method is not the focus of this report, so they are not reviewed further. However, the following sections summarize methods that have the potential to be used in coordination with energy absorbing approaches, such as those discussed in Section 2.

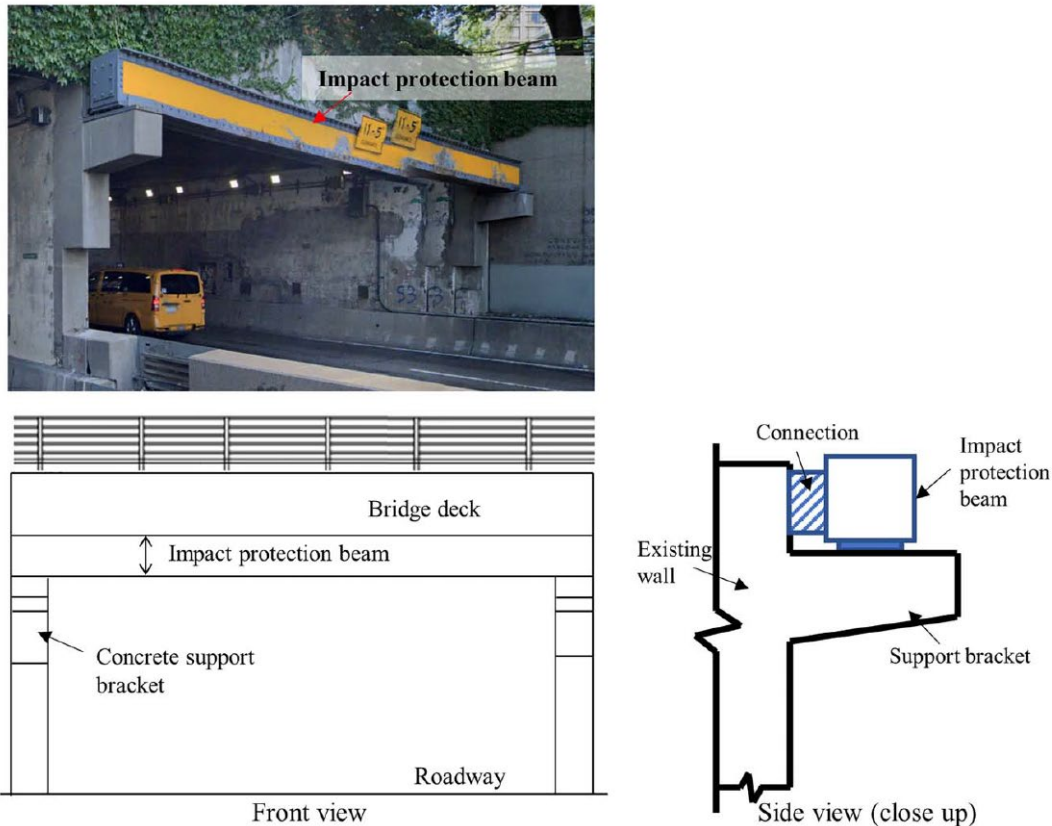
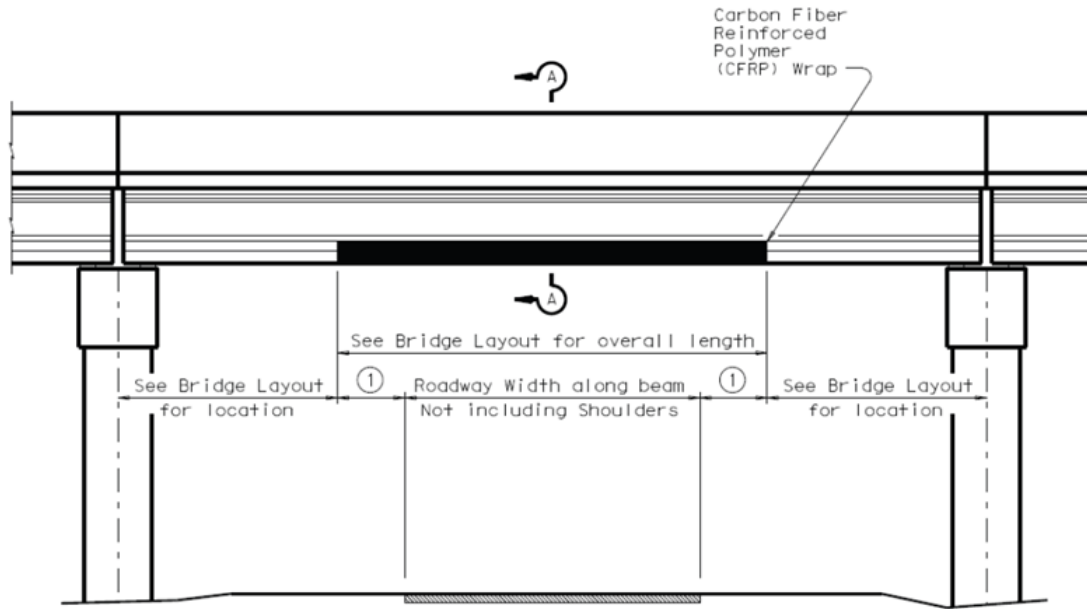


**Figure 29. Example beam for over-height vehicle protection (Cao, et al., 2023).**

#### 3.1. Bridge Protective Beam Wrap

TxDOT currently has a standard for a “Bridge Protective Beam Wrap” (BPBW) for over-height vehicle bridge impacts [ (Smith, 2014), (Nemec, 2013)]. It is intended for new construction for bridges with high probabilities of impact but can be used as a retrofit. Carbon fiber reinforced polymer (CFRP) wraps are placed on the bridge girder as shown in Figure 30 and Figure 31. Two layers of 24-inch (610 mm) wrap are used in the longitudinal and traverse directions as shown in Figure 31.



**TYPICAL BRIDGE ELEVATION**

*Figure 30. Bridge Protective Beam Wrap – Bridge Elevation (Smith, 2014).*

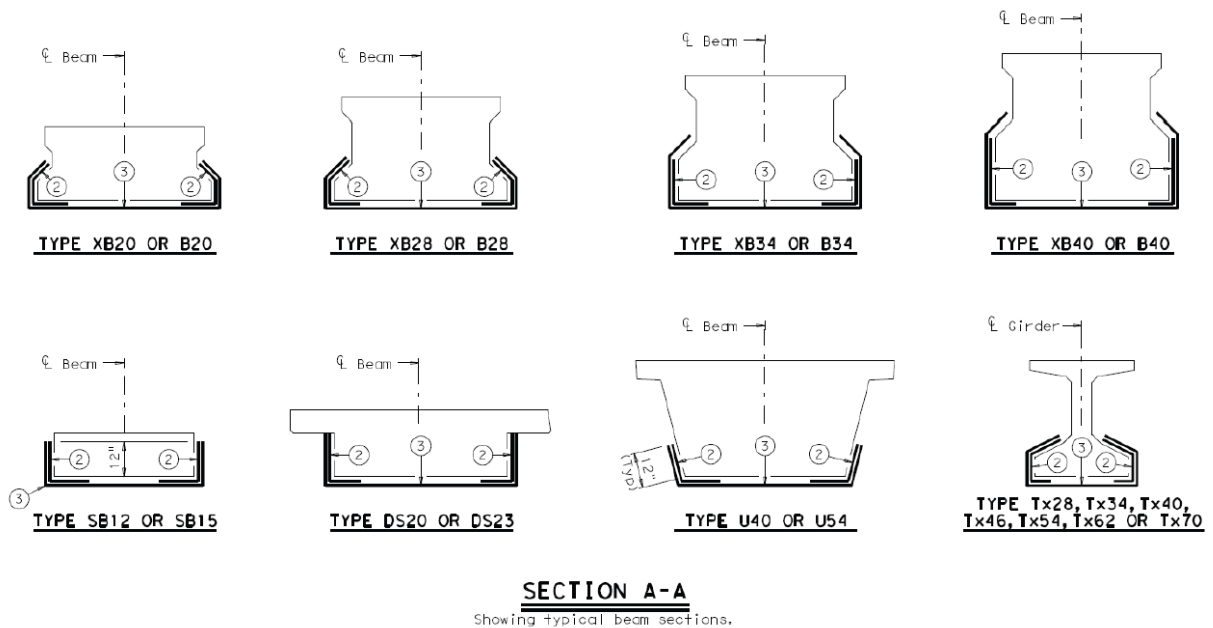


*Figure 31. Bridge Protective Beam Wrap – Girder cross sections (Smith, 2014).*

(Smith, 2014) described the benefits of the BPBW are that it reduces total damage to beams, concentrates the damage, and captures debris. No experiments or analysis were provided, but an image of damage from

a bridge girder strike was provided, as shown in Figure 32. The 2013 cost of the installation is \$49/ft<sup>2</sup> or approximately \$3900 for a 30-ft (9144 mm) girder.



*Figure 32. Bridge beam hit with BPBW installed (Smith, 2014).*

(Agrawal, El-Tawil, Cao, & Wong, 2022) subsequently performed an analysis of a BPBW installed by TXDOT. As mentioned in Section 2.1, the CFRP wrap did not sufficiently enhance the lateral capacity of the girder and it displayed significant damage. A photograph of actual damage to a girder from an over-height truck impact is shown compared with the FEA simulation result in Figure 33.

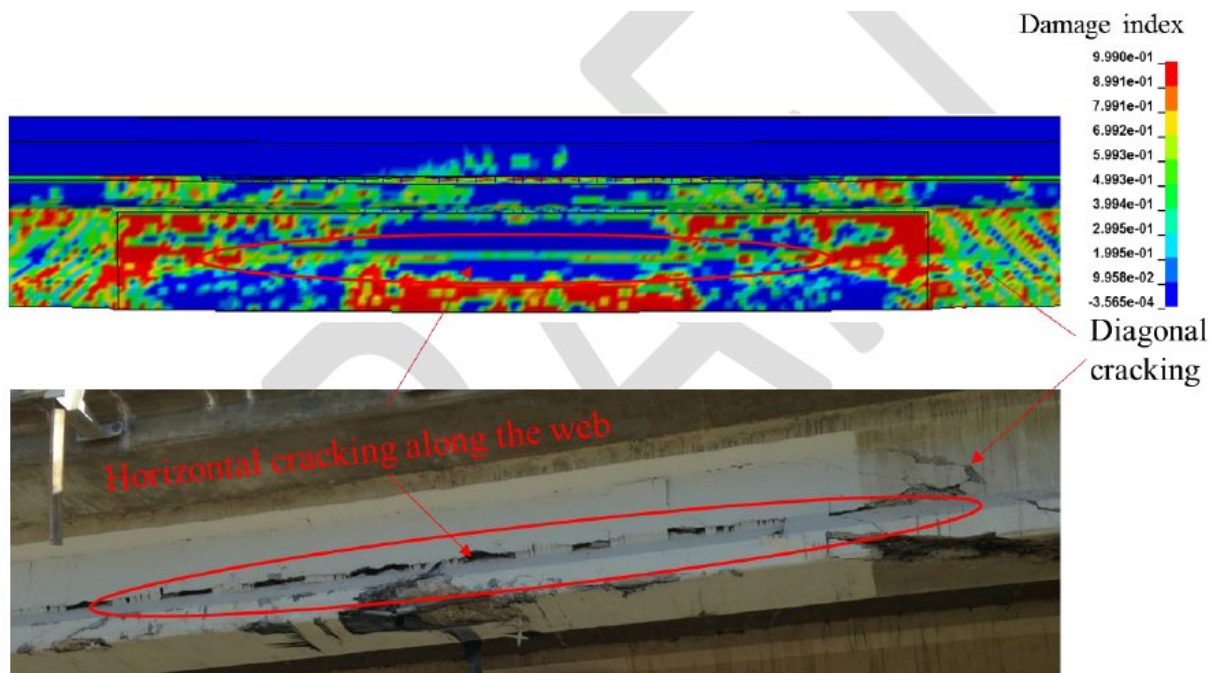


*Figure 33. Damage of the CFRP wrapped girder from over-height impact (Agrawal, El-Tawil, Cao, & Wong, 2022).*

### 3.2. Hybrid Composite Beam

(Jing, 2017) performed full-scale experimental and analytical studies to evaluate the dynamic behavior of PC and Hybrid Composite Beam (HCB) bridge girders under lateral impact from over-height vehicles. The HCB was developed for the construction of new and replacement bridges in rail infrastructure. The general

construction is shown in Figure 34. The main components are a concrete arch, steel reinforcement, a low-density foam core, and a fiber reinforced polymer (FRP) shell. The PC girder used in testing for comparison with the response of the HCB girder is shown in Figure 35.

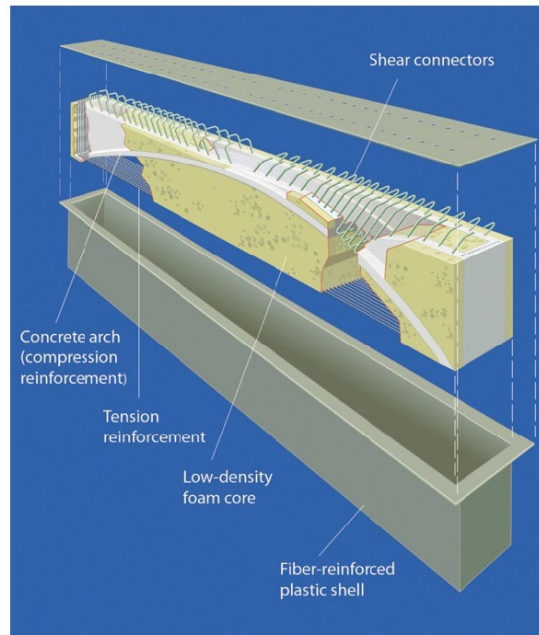


Figure 34. Hybrid composite beam (Hillman, 2012).

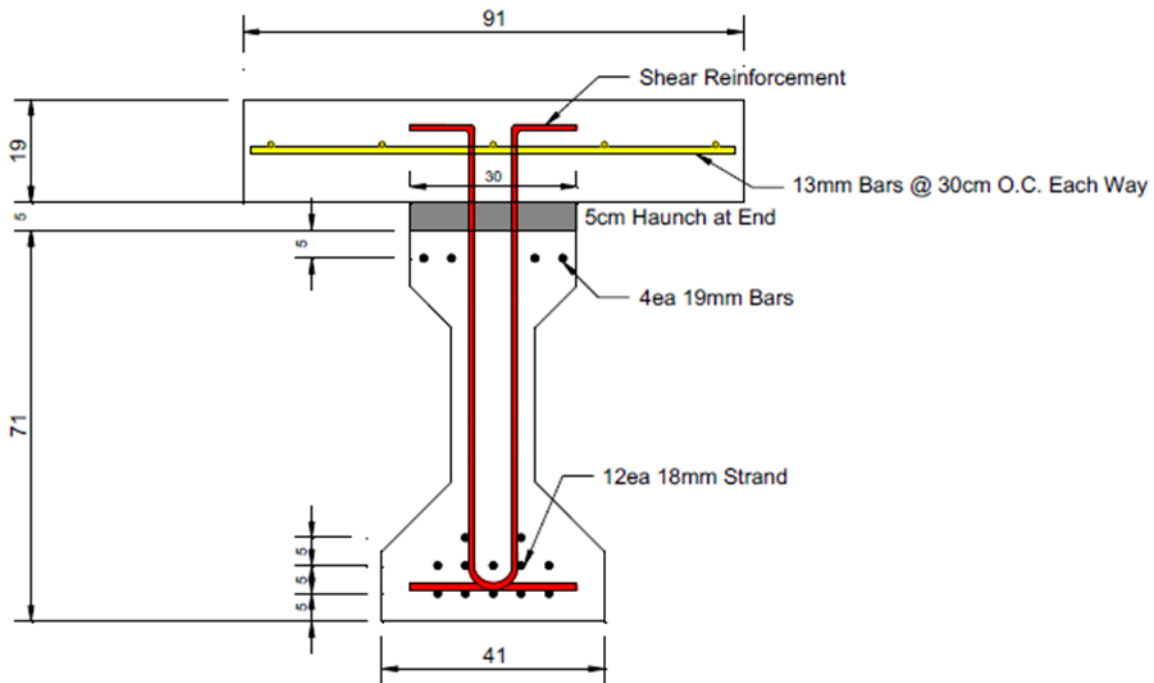


Figure 35. Cross section of PC girder (Jing, 2017).

A full-scale lateral impact test was performed on each girder using the setup shown in Figure 36. An impact cart weighing 9000 lb (4082 kg) rolled down the track and impacted a test article at a speed of 15 mph (24 km/h) and 96 kJ impact energy (709 kip-ft). The impact cart is made of a steel box filled with concrete and impacts the bottom of the girder. A complete test article with an HCB girder attached to a portion of a bridge deck is shown in Figure 37 and with the PC girder in Figure 38. Note that the bridge deck component of the test article is different in the two tests.



*Figure 36. Full-scale lateral impact test setup (Jing, 2017).*



*Figure 37. Full-scale lateral impact test article with HCB shown (Jing, 2017).*

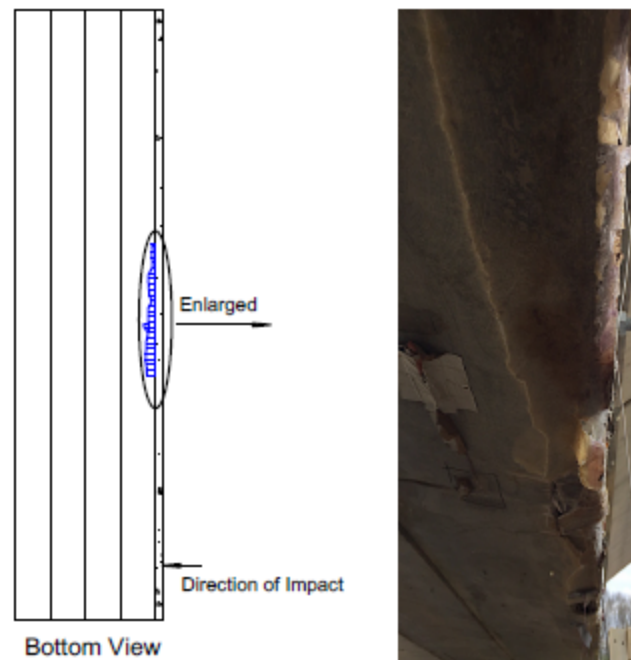


*Figure 38. Full-scale lateral impact test article with PC girder shown (Jing, 2017).*

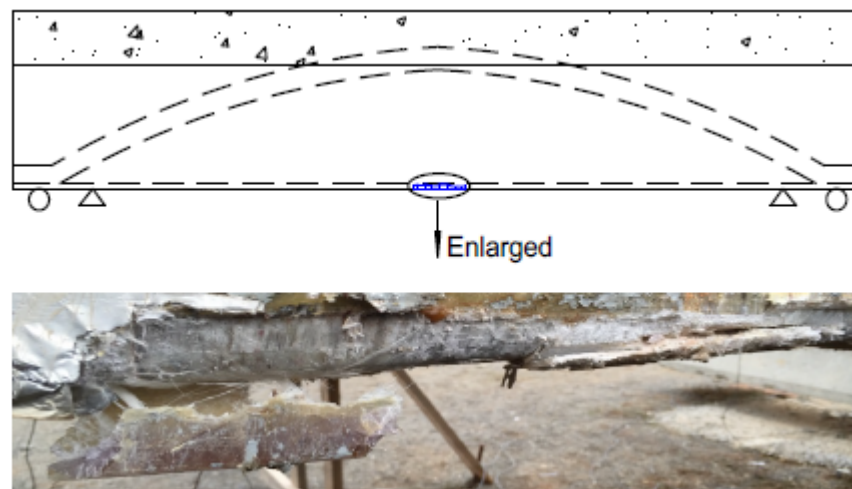
Impact with the PC girder resulted in global failure of the girder that began with punching shear around the impact zone. The impactor then penetrated further, and the damaged impact zone behaved as a “hinge” with global motion of the girder. The final damaged girder is shown in Figure 39. The HCB girder, however, experienced no global failure. There was local damage of the FRP shell around the impact zone with large cracks, debonding of the shell from the foam and tearing of the FRP shell, as shown in Figure 40. The authors noted that a lot of energy was absorbed through local strain energy of the tension reinforcement and the low-density foam and that the resilient nature of the materials around the impact zone makes an HCB bridge girder an effective structure to resist lateral impact loading.



*Figure 39. PC girder after the impact test (Jing, 2017).*



(a) Bottom face



(b) Front face

**Figure 40. HCB girder after the impact test (Jing, 2017).**

The authors also noted that several repair methods were suggested by (Hillman, 2012):

- Vacuum infusion of vinyl ester by drilling several holes in the laminate can be adopted to restore the bond between FRP laminas and between FRP shell and interior foam.
- In damaged areas with obvious cracks, the FRP laminate should be cut off the structure and new FRP strengthening patches should be applied to these areas.

## 4. Over-height Collision Impact Loading and Analysis Methods

Over-height vehicle impacts cause a range of damage to bridges from minor damage, requiring minimal repair, to severe impact shear cracking patterns, requiring replacement. Examples are depicted in Figure 41 (Harries, Kasan, Miller, & Brinkman, 2012). Characterization of the nonlinear dynamic nature of over-height collision involves assessment of the impact loading from the vehicle, the girder response and material behavior.

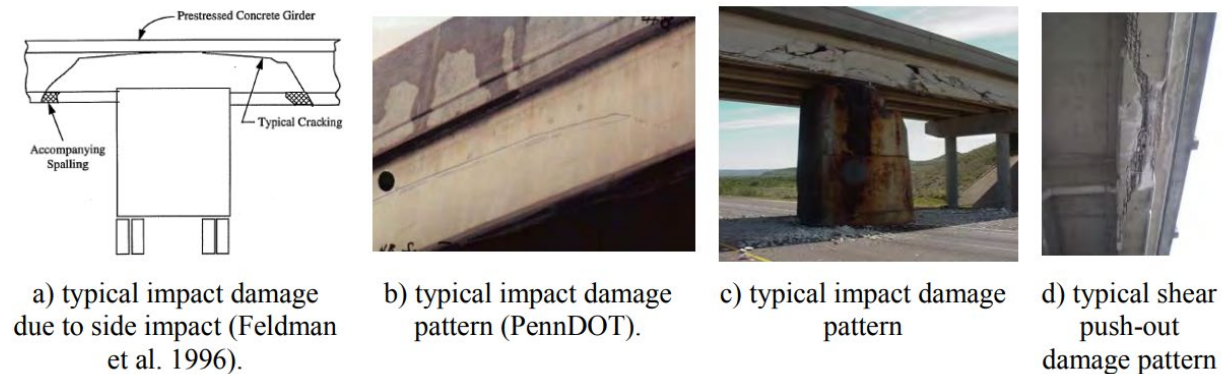


**Figure 41. Typical impact damage from over-height collisions (Harries, Kasan, Miller, & Brinkman, 2012).**

There is some guidance in existing standards for static design loading on bridges due to vehicular impact. There are also recent studies that developed analytical models to define loading on bridge girders from over-height vehicles. The authors evaluated the equivalent static force, dynamic impact force, force history and demand models to be applied to the girders. Computational models for the vehicles, cargo, and girders are used to define the loading and evaluate the response of the girder, bridge deck, and proposed protection systems. The following sections provide a summary of these three methods.

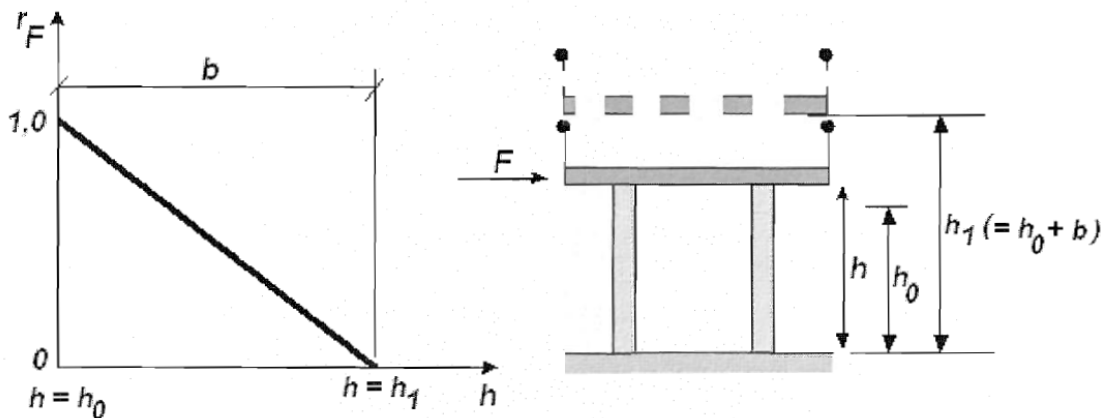
### 4.1. Bridge Impact Loading Specified in Industry Standards

Current industry standards for impact loads on bridges include AASHTO Load and Resistance Factor Design (LRFD) Bridge Design Specifications (AASHTO, 2017) and European Standard EN 1991-1-7:2006: E (CEN, 2006). The AASHTO LRFD specification calls to apply a design force of 600 kips (2669 kN), but this is only for piers or abutments. This value was derived from full-scale crash tests of an 80-kip (359 kN) tractor trailer impacting a rigid column at 50 mph, so it does not apply to superstructures of the bridge.

Section 4.3.2 Impact on Superstructures in EN 1991-1-7:2006:E provides design values for impact from lorries and/or loads carried by the lorries on superstructures. The indicative static design forces are provided in Table 11. Note that different forces are specified depending on the traffic category. A reduction factor in force is allowed depending on the bridge deck clearance above the road, as shown in Figure 42.

**Table 11. Indicative equivalent static design forces due to impact on superstructures (CEN, 2006).**

Category of Traffic	Equivalent Static Design Force
Motorways and country national and main roads	500 kN (112 kip)
Country roads in rural areas	375 kN (84 kip)
Roads in urban area	250 kN (56 kip)
Courtyards and parking garages	75 kN (17 kip)



AC1  $h$  is the physical clearance between the road surface and the underside of the bridge deck at the impact point

$h_0$  is the clearance between the road surface and the underside of the bridge deck, below which an impact on the superstructure need to be taken into account without any reduction. The recommended value of  $h_0$  is 5,0 m (+ allowances for vertical sag curve and deflection of the bridge, and expected settlements)

$h_1$  is the clearance between the road surface and the underside of the bridge deck, above which no impact need to be considered. The recommended value of  $h_1$  is 6,0 m (+ allowances for future resurfacing, vertical sag curve and deflection of the bridge, and expected settlements). AC1

$b$  is the difference in height between  $h_1$  and  $h_0$ , i.e.  $b = h_1 - h_0$ . The recommended value for  $b$  is 1,0 m. A reduction factor for  $F$  is allowed for values of  $b$  between 0 and 1 m, i.e. between  $h_0$  and  $h_1$ .

**Figure 42. Reduction in static design forces accounting for bridge deck clearance (CEN, 2006).**

#### 4.2. Peak and Average Impact Force from a Box Truck Impact on a PC Box Girder

(Jing, Zhang, Zhou, Zhao, & Li, 2023) conducted a parametric FEA study on a PC box girder bridge impacted by an over-height two-axle truck shown in Figure 43. The study varied six factors to evaluate their influence on the impact load: girder configuration, vehicle speed, vehicle mass, impact angle, and concrete strength and prestress of the strand. Table 12 lists how the six factors were varied and Table 13 shows a general summary of the influence of each of these individual factors.

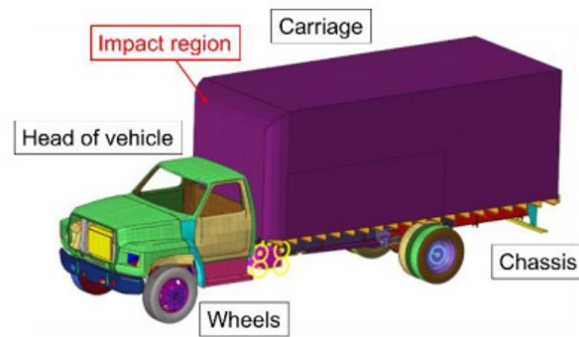


*Figure 43. Finite Element Model of the Truck Impactor (Jing, Zhang, Zhou, Zhao, & Li, 2023).*

*Table 12. Varied Conditions for the Parametric Analysis from (Jing, Zhang, Zhou, Zhao, & Li, 2023)*

Condition	Girder Configuration	Vehicle Speed (km/h)	Vehicle Mass (t)	Impact Angle (°)	Concrete Strength	Ultimate Tensile Strength of Strand (MPa)
1	Box girder	80	20	0	C50	1860
2	Hollow slab	80	20	0	C50	1860
3	T-shaped girder	80	20	0	C50	1860
4	Box girder	40	20	0	C50	1860
5	Box girder	60	20	0	C50	1860
6	Box girder	80	10	0	C50	1860
7	Box girder	80	30	0	C50	1860
8	Box girder	80	20	15	C50	1860
9	Box girder	80	20	30	C50	1860
10	Box girder	80	20	0	C40	1860
11	Box girder	80	20	0	C60	1860
12	Box girder	80	20	0	C50	1570
13	Box girder	80	20	0	C50	1270

**Table 13. Influence of Individual Parameters on Over-height Vehicle Collision (Jing, Zhang, Zhou, Zhao, & Li, 2023)**

Parameter	Summary of Impact on Dynamic Behavior of Bridge
Girder Type	Box Girder Bridge: Smallest damage during collision, displacement at midspan of girder within 7mm
	T-girder Bridge: Greatest damage (local materials at impact and overall bridge displacement reaching maximum level)
	Hollow Slab Bridge: Plastic damage lies between the box and T-girder types
	Summary: Girder configuration has little effect on the maximum impact force generated
Vehicle Speed	40 km/h (25 mph): Plastic damage area is small with a small amount of concrete falling off
	60 km/h (37 mph): Expanded damage area with concrete on bottom flange falling off
	80 km/h (50 mph): Maximum damage area, Increased horizontal (38%) and vertical impact force (50%) from 40 km/h collision
	Summary: No damage was observed at the longitudinal rebars and stirrups at the impact area for all speeds. As speed increases, local damage at the impact area, impact force and midspan displacement also increase.
Vehicle Mass	10 and 15 tons: Small amount of concrete on the impact area is broken, no damage on opposite side
	20 and 30 tons: Concrete at the impact area and bottom flange of the girder falls off with large plastic damage opposite the impact area
	Summary: Increase in vehicle mass increases the impact force and displacement of the bridge
Impact Angle	0°: Concrete at the impact area of the side girder fell off with no damage occurring on the rebars
	15°: Plastic damage extends to the bottom flange of the girder with the rebars at the bottom flange being ruptured
	30°: Damage degree increases with more rebars being ruptured
	Summary: Increasing the impact angle increases the midspan displacement and decrease the impact force
Concrete Strength	Summary: Concrete strength only has a certain influence on the plastic damage of the local vehicle impact region with no effect on the dynamic response of the bridge
Strand Pre-stress	Summary: Prestress of the strand only has a certain influence on the damage of the local vehicle impact region with no effect on the dynamic response of the bridge

A function was derived to describe the peak and average impact force that accounts for the influence of impact angle and mass

$$F = av^b m^c (1 + d\theta + e\theta^2 + fm\theta) \quad (2)$$

where  $m$  is vehicle mass (tons),  $v$  is velocity (km/h),  $\theta$  is the impact angle (rad) and  $d$ ,  $e$ , and  $f$  are fit parameters. The associated parameters are given in Table 14. These values are static design loads, and a corresponding pulse loading is not given. The results of this parametric study showed that the peak and mean impact force was independent of girder type, concrete strength, and strand pre-stress.

**Table 14. Fit Parameters to the Impact Force Formula (Note if the impact angle is zero, then  $d$ ,  $e$ , and  $f$  are set to zero.)**

Impact Force (MN)	$a$	$b$	$c$	$d$	$e$	$f$
Peak Impact Force	0.07	0.502	0.224	-0.377	0.137	0.007
Average Impact Force	0.099	0.227	0.082	-2.745	2.118	0.044

#### 4.3. Demand Model for Varied Stiffness Cargo on a Semi-Trailer Truck

(Cao, et al., 2023) and (Agrawal, El-Tawil, Cao, & Wong, 2022) developed a demand model from FEA simulations of three types of cargo pulled by a semi-trailer truck: soft, semi-rigid, and rigid. The objective of this model is that the specified force pulse causes the same displacement to the impacted beam as that from the FEA model of the truck (Agrawal, El-Tawil, Cao, & Wong, 2022). The authors provided a description for the various cargo these models are meant to represent as described in Table 15. The tractor semi-trailer models used in this analysis are discussed further in Section 4.6.1. The demand function derived from the simulations suggests use of a pulsed loading that accounts for the impactor stiffness, as shown in Figure 44. The recommend pulse is based on the type of cargo impacting the girder. The equation for the demand function was fit for a certain range of truck velocities and weights [i.e., 64 to 113 km/h (40 to 70 mph) and 180 to 360 kN (405 kip to 809 kip), respectively, and beams depths ranging from 0.864 to 1.168 m (2.83 to 3.83 ft).

**Table 15. Examples for Representative Tractor Semi-trailer Types (Cao, et al., 2023)**

Cargo	Examples
Soft	Regular trailers (made of thin plywood, aluminum, and steel sheets)
Semi-rigid	Modular steel structures, e.g., components for oil field work
Rigid	Backhoe/excavators and rigid machines

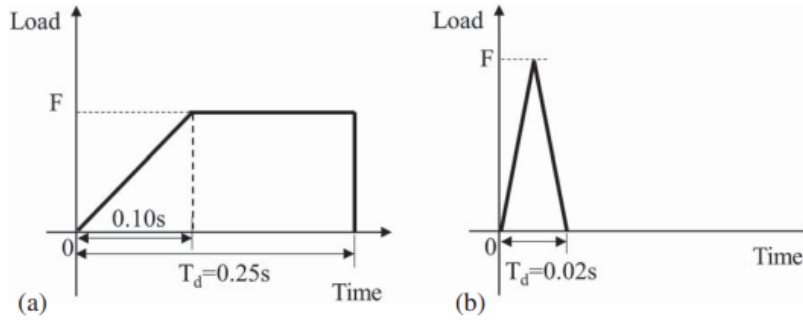


**Figure 44. Proposed impact force demand model (a) ramped pulse for the soft case (b) triangular pulse for the semi-rigid and rigid case (Cao, et al., 2023).**

The proposed impact force is

$$F = \begin{cases} 44.84V^{0.7} & (\text{soft}) \\ 0.042V^{0.79}W^{1.35}C^{0.15} & (\text{semi-rigid}) \\ 0.082V^{0.92}W^{1.13}C^{0.26} & (\text{rigid}) \end{cases} \quad (3)$$

where  $V$  is the truck velocity (km/hr) and  $W$  the truck weight (kN). The plastic capacity (kN) of the impacted beam is

$$C = 2 \frac{M_p}{0.5(L_3 - L_2)} \quad (4)$$

where  $M_p$  is the plastic moment of the steel beam,  $L_3$  is the beam span, and  $L_2$  is the width of the trailer cargo. The plastic capacity of the beam is based on the plastic-hinge assumption. The relationship was obtained using regression analysis with varied truck types, velocity, and beam depths. (Agrawal, El-Tawil, Cao, & Wong, 2022) notes that these demand equations are similar to that for impact of trucks on piers in (AASHTO, 2017), (Agrawal, et al., 2018), (Cao, Agrwal, El-Tawil, Xu, & Wong, 2019), (Xu, Cao, El-Tawil, Agrawal, & Wong, 2019).

This impact force is applied to an impacted girder as shown in Figure 45 where  $L$  is defined as the length of the loading area based on the impactor type: 2.4 m (soft), 2.4 m (semi-rigid), and 1.8 m (rigid). Note Figure 45 implies the force is applied over the full height, although the authors do not explicitly state this fact.

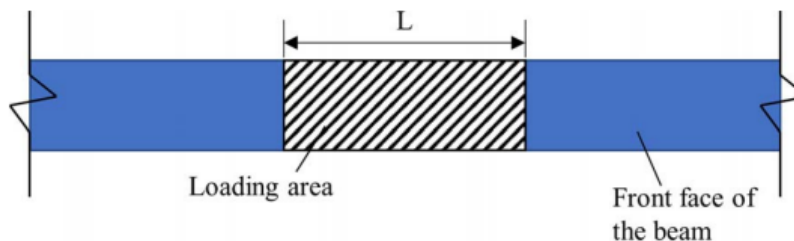


**Figure 45. Loading application of the demand model (Cao, et al., 2023).**

#### 4.4. Demand Equation for Varied Impactors on AASHTO Bridge Girders

(Oppong, Saini, & Behrouz, 2021) performed parametric FEA to characterize the impact force, internal shear, and damage pattern on AASHTO Type I and AASHTO Type IV bridge girders from varied types of impacting objects: concrete pipe, steel tank, PVC pipe, wooden-box container, and a trailer of a semi-truck on. These impactors are shown in Figure 46. A range of forces are given at 72 km/h (45 mph) and 120 km/h (75 mph) for all the impactors in Figure 47 and Figure 48. In Figure 48, the forces are given for different lengths of the impacting objects, listed as a fraction of their base lengths. The peak dynamic impact force for the concrete pipe on the Type IV girder, for example, is about 20,000 kN (4496 kips). The authors then developed equations for the peak and mean force from the concrete pipe and the steel tank as a function of their geometry and speed.

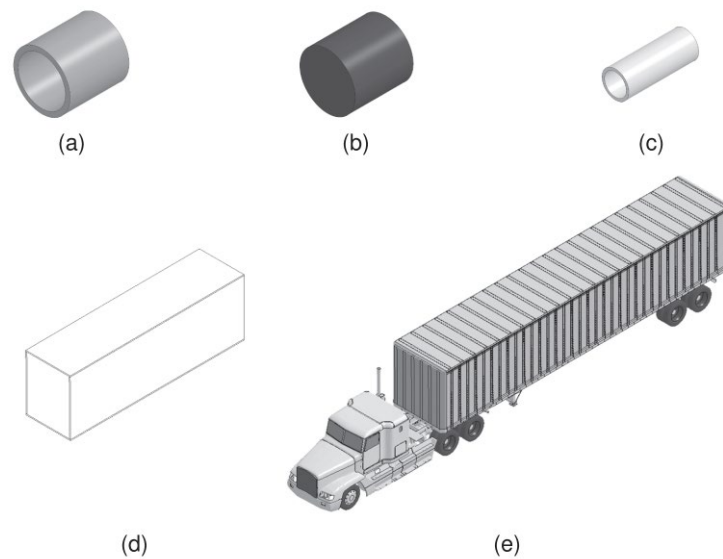


**Figure 46.** Types of impactors used in (a) concrete conduit pipe, (b) cylindrical steel tank, (c) PVC pipe, (d) wooden box container, (e) tractor semi-trailer (Oppong, Saini, & Behrouz, 2021).

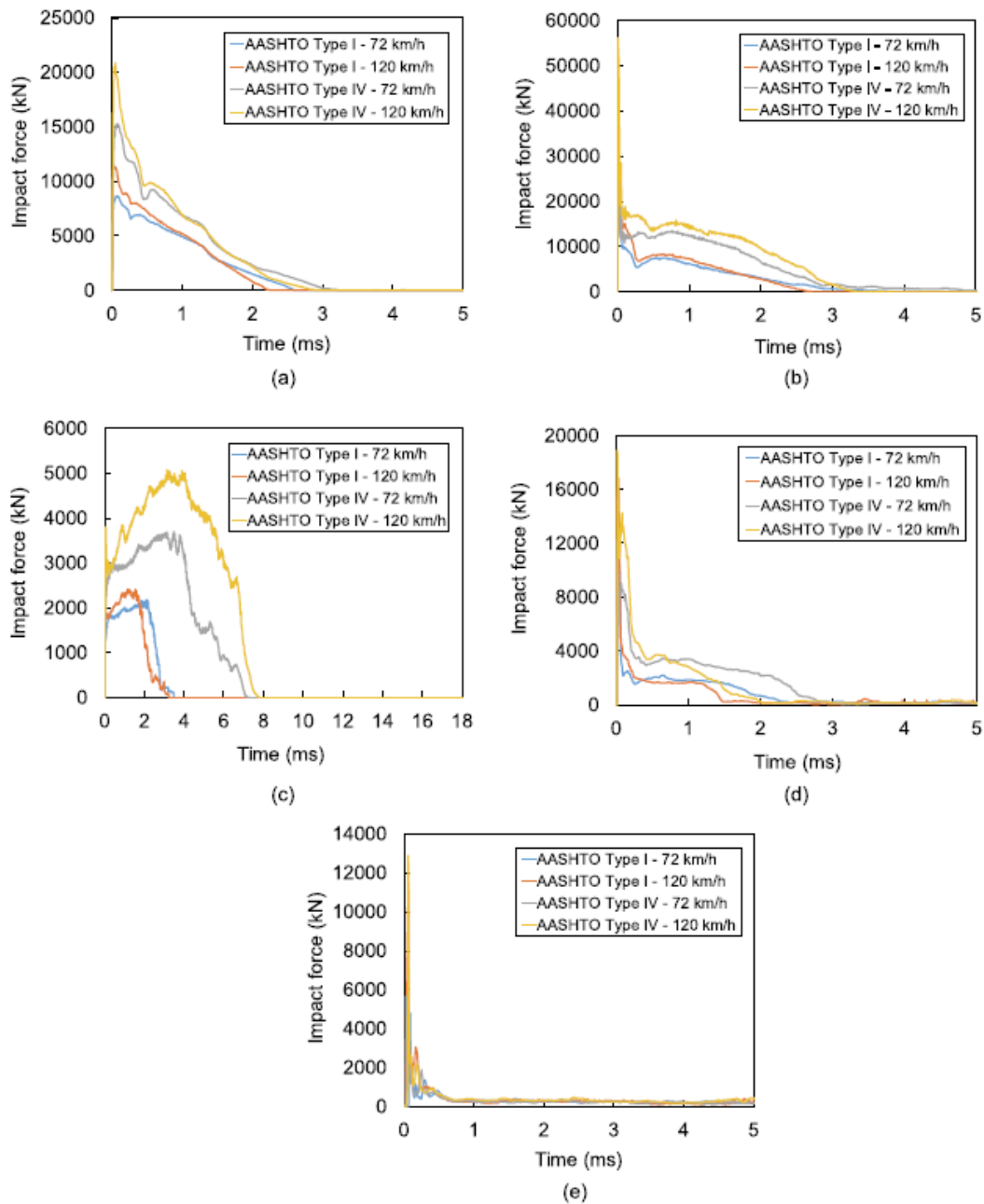
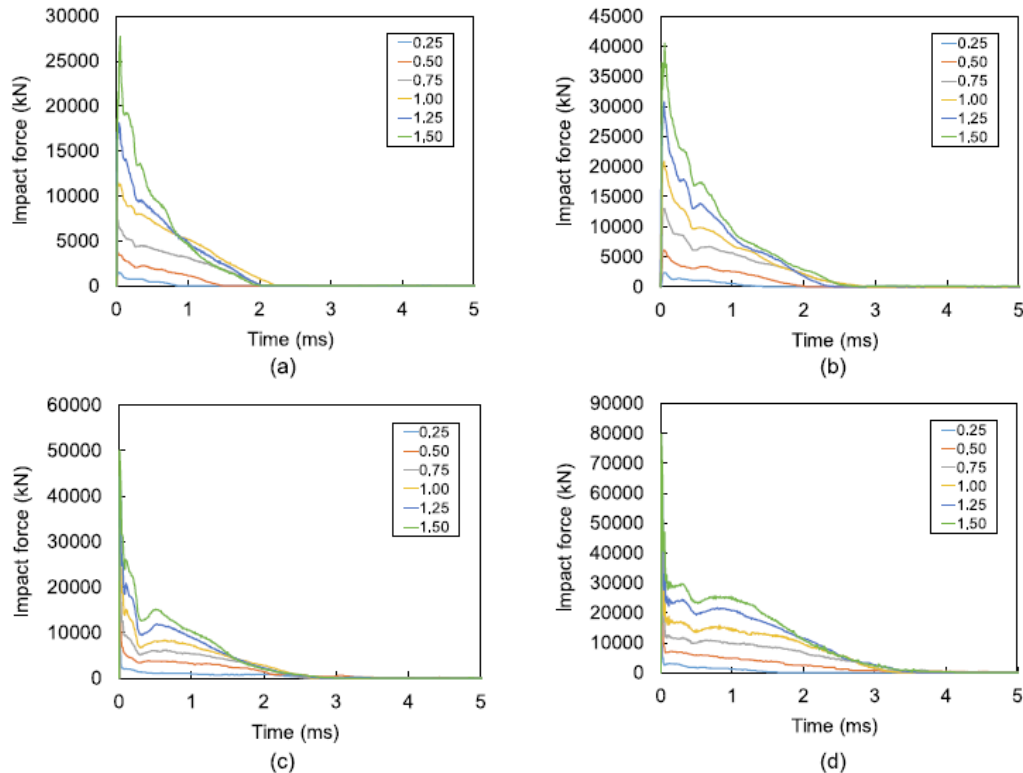


Figure 47. Impact force history on AASHTO girders from collisions with (a) concrete pipe (b) steel tank (c) PVC pipe (d) wooden box (e) tractor-semitrailer (Oppong, Saini, & Behrouz, 2021).



**Figure 48. Impact force time history for various sizes of impacting objects traveling at a velocity of 120 km/h (75 mph): (a),(b) concrete pipe (c),(d) steel tank into Type I and Type IV girders (Oppong, Saini, & Behrouz, 2021).**

#### 4.5. Analytical Design Methods Using Crushable Sandwich Structures

(Yang M. , 2006) and (Qiao, Yang, & Mosallam, 2004) developed simplified analytical models to approximate the impact response of the I-Lam system discussed in Section 2.3. These models were developed to quickly perform design optimization. The impact scenario is first simplified as shown in a free-body diagram shown in Figure 49 where the shear-off mechanism of the over-height portion of the truck has a mass  $M_s$  and shear-off stress of  $\tau_w$  and area  $A_s$ . The shear-off portion is the part of the truck that breaks away during impact. The truck mass is  $M_T$  and  $P_c$  is the contact force between the shear-off portion and the sandwich beam. The  $V_0$  is the initial velocity of the truck.

The I-Lam honeycomb structure with facesheets is modeled with the mechanical analog shown in Figure 50. In the model,  $M$  is the mass of the impactor;  $m$  is the mass of the top face sheet in the sandwich beam;  $w_1$  and  $w_2$  are the displacements, respectively, of the over-height portion of the truck and the top face sheet of the sandwich;  $K_c$  is the contact stiffness;  $K_{bs}$  is the combined bending a shear stiffness of the top face sheet of the sandwich;  $K_{core}$  is the through-thickness stiffness of the core;  $K_m$  is the stiffness contributed by the membrane effect of the face sheet.

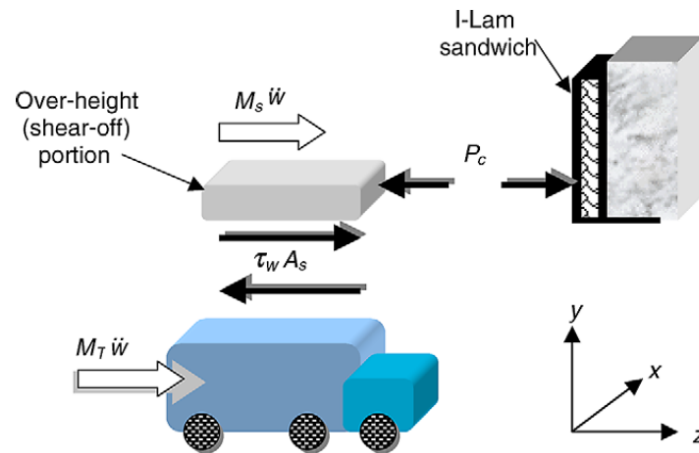


Figure 49. Free-body diagram of the shear-off of an over-height portion of a truck (Qiao, Yang, & Mosallam, 2004).

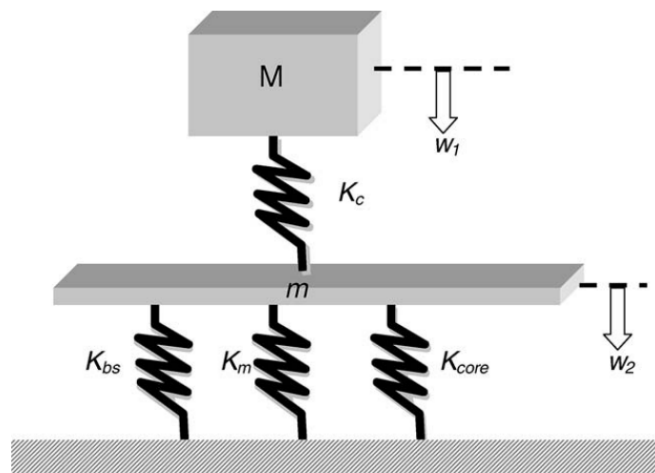


Figure 50. Discrete model of rigidly supported sandwich beam under impact (Qiao, Yang, & Mosallam, 2004).

The authors present three types of loading cases for I-Lam structures: discrete impact loading, concentrated impact load, and distributed impact load. The discrete impact loading is for when the I-Lam sandwich panel is impacted by a moving truck. The equation below represents the closed form solution for the contact force and duration,  $T_c$ , where  $t$  is time and  $t < T_c$  indicates that the truck and I-Lam sandwich are in contact.

$$\begin{cases} P_c = V_0 \sqrt{K_{eq}} M \sin \sqrt{\frac{K_{eq}}{M}} t \\ T_c = \frac{\pi}{\omega} = \pi \sqrt{\frac{M}{K_{eq}}}, t < T_c \text{ (objects in contact)} \\ \omega^2 = \frac{K_{eq}}{M}, K_{eq} = \frac{(K_{bs} + K_{core}) K_c}{(K_{bs} + K_{core} + K_c)} \end{cases} \quad (5)$$

The over-height truck impacting the I-Lam will cause the initial contact force due to shear-off of the I-Lam. The above equation does not consider this shear-off effect. A closed form solution for the contact force and duration which accounts for the shear-off effect is

$$\left\{ \begin{array}{l} P_c = K_{eq} \left( \frac{V_0}{\sqrt{K_{eq}/M_s}} \sin \sqrt{\frac{K_{eq}}{M_s}} t - \frac{\tau_w A_s}{K_{eq}} \cos \sqrt{\frac{K_{eq}}{M_s}} t + \frac{\tau_w A_s}{K_{eq}} \right) \\ T_c = \frac{\pi}{\omega} = \pi \sqrt{\frac{M_s}{K_{eq}}} \end{array} \right. \quad (6)$$

where  $M_s$  is the mass of the shear-off portion and  $\tau_w$  is the shear strength of the over-height materials.

These analytical models were compared with finite element results from LS-DYNA. The stiffness parameters used in the analytical equations are given in Table 16. In comparison to the LS-DYNA models, the proposed analytical solutions compare relatively well with the contact force history. The discrete model shows a better correlation with finite element predictions compared as to the other two models. These models provide a basis for design of I-Lam sandwich structures.

**Table 16. Parameters used in the linear elastic analytical model (Qiao, Yang, & Mosallam, 2004).**

Parameter	Value
$K_c$ (N/m)	$1.54 \times 10^{10}$
$K_{core}$ (N/m)	$1.00 \times 10^8$
$K_{bs}$ (N/m)	$3.84 \times 10^6$
$\tau_w$ (Pa)	$1.0 \times 10^4$
$M_s$ (kg)	0.0361
$A_s$ (m <sup>2</sup> )	1.0
$V_0$ (m/s)	30

Finally, (Yang & Qiao, 2010) and (Yang M. , 2006) propose several design criteria to be used with this analytical model. The design procedure proposes three failure bounds: contact-force, deflection of the I-Lam, and energy-based design. The design failure criteria are listed in Table 17. The contact force is limited by the strength of the concrete,  $f'_c$ , in the impacted girder and A is the contact area. The I-Lam cannot deflect more than when the honeycomb reaches maximum density. Finally, the energy portion absorbed by the cushion material should be less than the maximum absorbing or crushing energy of the cushion. The  $U_{cushion}$  is the energy absorbed by the I-Lam,  $U_{kinetic}$  is the initial kinetic energy;  $W_{shear-hardening}$  is the work done by the shear hardening introduced by the over-height material;  $U_{residual}$  is the residual kinetic energy of the sheared-off material;  $U_{material}$  is the energy dissipated by the failure of the sheared-off material.

**Table 17. Design Criterion for Protective Sandwich Structures**  
(Yang & Qiao, 2010), (Yang M. , 2006).

Design Criteria	Equations	Explanation
Contact force	$P_c \leq f'_c A$	<ul style="list-style-type: none"> <li>• Contact force generated by the shear-off material (see Figure 50)</li> <li>• Only pure compressive failure considered for concrete</li> </ul>
Deflection	$\Delta_{max} \leq \Delta_{densification}$	The maximum deflection over the protective cushion should be less than the densification displacement of the protecting sandwich cushion
Energy	$U_{cushion} = U_{kinetic} + W_{shear-hardening}$ $-U_{residual} - U_{material} \leq U_{crushing}$	The kinetic energy generated by the projectile, or the sheared-off material are transferred to absorption by the cushion material, residual kinetic energy of the over-height material, and energy dissipated by deformation and failure of the projectile or sheared-off material itself. Based on the energy conservation, the energy portion absorbed by the cushion material should be less than the maximum absorbing or crushing energy of the cushion.

#### 4.6. Computational Methods

The most common method used for analysis of damage to bridge girders from over-height vehicle impacts and the protection provided by EA systems is through use of nonlinear dynamic FEA (e.g., LS-DYNA, Ansys Explicit), as was shown in

Table 1. This section provides a brief overview of the computational modeling methods used in these analyses, including the vehicle models used to apply loading to the bridge structures and details on the materials modeling implemented to predict the bridge structure response as well as the response of the EA systems.

##### 4.6.1. FEA Models of Vehicles Used for Analysis of Over-height Impact Events

A variety of types of over-height vehicles and cargo can impact a bridge girder. Researchers have applied different models in the study of protection systems and evaluating damage to different girder types. A summary of the vehicle/cargo models found in the literature is provided in Table 19.

The tractor-trailer model in models #1 to #3 was used by (Cao, et al., 2023) and (Agrawal, El-Tawil, Cao, & Wong, 2022) with the original model developed by (Plaxico, Miele, Kennedy, Simunovic, & Zisi, 2008), (Plaxico, Miele, Kennedy, Simunovic, & Zisi, 2009) and (Miele C. , Plaxico, Stephens, & Simunovic, 2010). This model was developed for use in analysis, design, and evaluation of roadside safety hardware and validated with full -scale crash tests with roadside barriers. (Agrawal, et al., 2018) and (Cao, Agrwal, El-Tawil, Xu, & Wong, 2019) modified the trailer to represent other impact structures and apply different

impact forces, or demand models, on the bridge girders. The first (model #2- ‘semi-rigid’) was developed to model the Skagit River bridge collapse where the trailer carried a cargo made of a reinforced container-like structure without side panels, as described in (Cao, Agrawal, El-Tawil, & Wong, 2021). To emulate rigid machines, a rigid block with dimensions of 2.0 m × 2.5 m × 1.8 m (6.6 ft x 8.2 ft x 5.9 ft) was attached to the flat bed of the trailer in model #3. The authors provided examples of their interpretation of each cargo type, as shown in Table 18

*Table 18. Examples of cargo types used with model #1 (Cao, et al., 2023).*

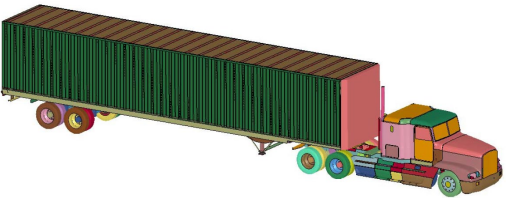
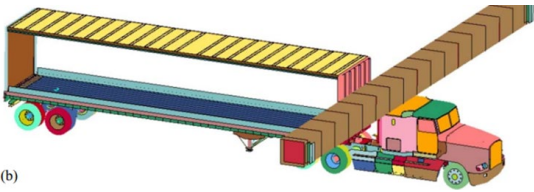
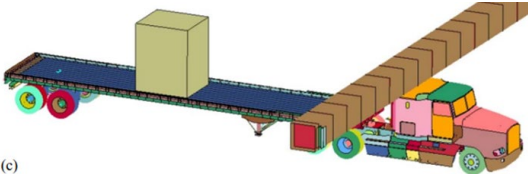
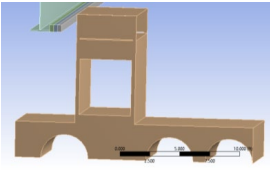
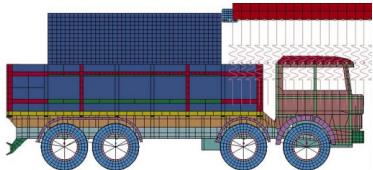
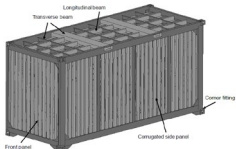
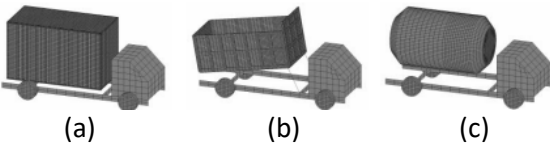
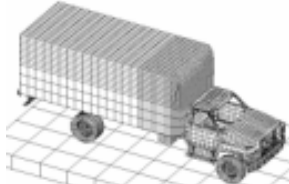
Cargo Type	Examples
S	Regular trailers (made of thin plywood, aluminum, and sheets)
SR	Modular steel structures (e.g., components for oil field work)
R	Backhoe/excavators and rigid machines

Model #4 is a relatively simple model made to emulate a semi-truck where the wind deflector impacts a girder. The truck is a rigid body with estimated inertial properties and the wind deflector is approximated as thin sheet metal with a perfect connection to the rigid body. Model #5 is a 30,000-kg (66,139 lb) IVECO truck developed by (Atahan, Bonin, & M., 2007) and used by (Sharma & Hurlebaus, 2012) for girder impact analysis. This model was validated using crash tests against steel and concrete barriers. The cargo used by (Sharma & Hurlebaus, 2012) is not in the original model, however, and no discussion is provided on its characteristics.

The standard shipping container model #6 was developed by Sha, Y., et al. (2020) and used by (Dyrkolbotn, 2021) for over-height impact of steel bridge girders in ship collisions. This is a detailed FEA model of a 5.97 m x 2.43 m x 2.82 m (19.6 ft x 7.97 ft x 9.25 ft) container with a frame structure made of top and bottom rails, corner posts and fittings, and transverse and longitudinal beams with corrugated front and side panels, floors, and top structure.

(Xu L., Lu, Guan, & Zhang, 2013) developed FEA models for three ‘typical Chinese vehicles’: Dongfeng 145 container truck, Dongfeng 3208 tipper truck, and Dongfeng EQ140 with a cement tank (model #7). These models were used to evaluate impacts with PC bridge structures, but no description of their development or validation are provided. The same authors used a Ford F800 FEA model #8 for the same analyses. This model was developed by (Miele C. , Plaxico, Kennedy, Simunovic, & Zisi, 2005) and validated with crash tests against roadside barriers. There is no mention of validation for the overhead structure of this model.

Table 19. FEA Vehicle or Cargo Models used for Bridge Girder Impact Analysis.

#	Author (s)	Vehicle Type	Model
1	(Miele C. , Plaxico, Stephens, & Simunovic, 2010)	Tractor-trailer (plywood, aluminum, and steel sheets) - S	
2	(Cao, et al., 2023)	Tractor-trailer Trailer modular steel (e.g., components for oil field work) - SR	 (b)
3	(Cao, et al., 2023)	Tractor-trailer Flatbed with rigid cargo - R	 (c)
4	(Aly & Hoffmann, 2022)	Semi-truck Wind deflector deformable Truck rigid body	
5	(Atahan, Bonin, & M., 2007)	30,000 kg IVECO Truck	 (Sharma & Hurlebaus, 2012)
6	(Sha, 2021)	20-ft standard shipping container	 (Dyrkolbotn, 2021)
7	(Xu L. , Lu, Guan, & Zhang, 2013)	Typical Chinese vehicles (a) Dongfeng 145 container truck (b) Dongfeng 3208 tipper truck (c) Dongfeng EQ140 cement tank	 (a) (b) (c)
8	(Miele C. , Plaxico, Kennedy, Simunovic, & Zisi, 2005)	Ford F800	 (Xu L. , Lu, Guan, & Zhang, 2013)

#### 4.6.2. Materials Modeling

Accurate modeling of material constitutive and failure behavior in nonlinear dynamic FEA is an essential part of impact analyses of all types, including that of bridge girders. Appropriate models are highly material dependent. Fortunately, there are many mature and validated constitutive models available in commercial FEA codes (e.g., LS-DYNA, Ansys Explicit Dynamics, Abaqus/Explicit) that can model many of the materials of interest in over-height vehicle impact analysis of bridge girders, including concrete, steel, honeycomb, foams, and other metals like aluminum. The open literature has extensive examples of accurate materials modeling for crash and impact applications where experiments and simulations show excellent agreement when performed by adept analysts and experimentalists that include the appropriate mechanics in their models and testing. A full review of the modeling performed, and testing required is well beyond the scope of this literature summary. This section provides a very brief overview of the types of constitutive modeling used for materials of interest in impact analysis of bridge girders.

Impact analyses of RC bridge structures are commonly modeled with explicit geometry defined for the concrete and reinforcing bars. An example for a RC box girder is shown in Figure 51 which was evaluated for damage due to impacts using the Ford F800 vehicle model (#8) discussed in the previous section. A variety of concrete constitutive models are used in analyses of this type, but all generally include geologic cap-types of strength models to account for variations in strength depending on the stress state in the material. Most models account for rate effects on strength. For example, (Jing, Zhang, Zhou, Zhao, & Li, 2023) used \*MAT\_CSCM\_CONCRETE in LS-DYNA for their simulations with a dynamic increase factor on the tensile and compressive strength from (Hao & Hao, 2014) and (Cheng & Qiao, 2015). As mentioned previously, most EA systems for bridge girders discussed in Section 2 were evaluated using nonlinear dynamic FEA using these approaches.

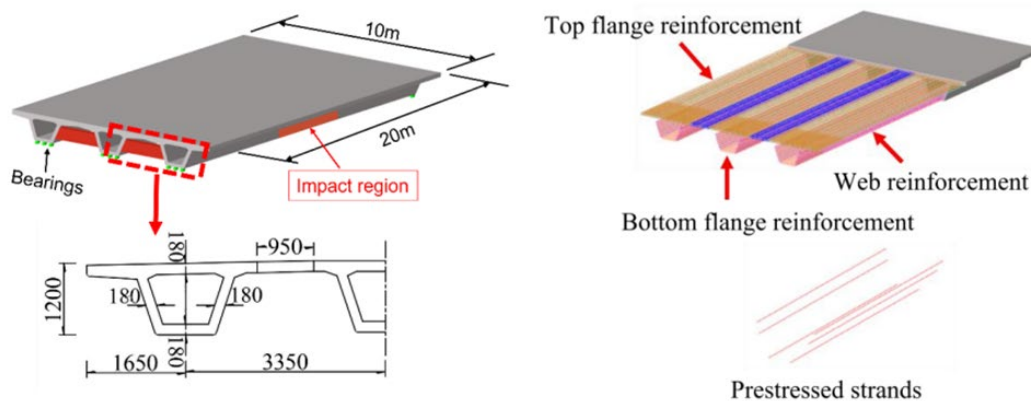


**Figure 51. Example FEA model of RC girder for over-height vehicle impact analysis (Jing, Zhang, Zhou, Zhao, & Li, 2023).**

Steel and aluminum are generally modeled in nonlinear FEA impact analyses using plasticity models that include isotropic and kinematic hardening and strain rate effects on yield and ultimate strength. There are a variety of models used for this purpose in explicit FEA codes. (Xu L. , Lu, Smith, & He, 2012) for example, modeled over-height impact using a cylindrical tank with a counterweight to represent the truck and uses a Cowper-Symonds model for the steels (Livermore Software Technology, 2021). The reinforcing bars in a AASHTO Type I and IV girders were modeled using a Piecewise Linear Plasticity model (Livermore Software Technology, 2021) by (Oppong, Saini, & Behrouz, 2021) to evaluate damage from a variety of over-height cargo. The vehicle FEA models themselves implement the same or similar models for their structures.

Honeycomb and crushable foam materials require specialized constitutive models that account for directional stiffness, crushing and shear strengths. LS-DYNA (Livermore Software Technology, 2021), for example, has several constitutive models that have been applied for these types of materials, including \*MAT\_CRUSHABLE\_FOAM, \*MAT\_HONEYCOMB, \*MAT\_SIMPLIFIED\_RUBBER/FOAM and \*MAT\_TRANSVERSELY\_ANISOTROPIC\_CRUSHABLE\_FOAM, [e.g., (Jackson, Fasanella, Annett, & Polanco, 2012)] and \*MAT\_LOW\_DENSITY\_FOAM, used by (Sharma, Hurlebaus, & Gardoni, 2008) to develop the bridge girder protection system discussed in Section 2.5, among others.

## 5. References

- AASHTO. (2017). *AASHTO LRFD Bridge Design Specification, 8th Edition*. Washington, D.C.: American Association of State Highway and Transportation Officials (AASHTO).
- Abu-Hajar, O. (2024, January 21). ODOT MSCE-Structures, Email correspondence.
- Abu-Odeh, A. (2008). Modeling and Simulation of Bogie Impacts on Concrete Bridge Rails Using LS-DYNA. *Proceedings of 10th International LS-Dyna Users Conference* (pp. 9-20). Livermore Software Technology Corporations.
- Agrawal, A., El-Tawil, S., Cao, R., & Wong, W. (2022). *Implementation of crash simulation technology to develop countermeasures strategies for over-height impact protection system on concrete girders, FHWA-RC-22-0003*. McLean, VA: Federal Highway Administration.
- Agrawal, A., El-Tawil, S., Cao, R., Xu, X., Chen, X., & Wong, W. (2018). *A Performance-Based Approach for Loading Definition of Heavy Vehicle Impact Events, FHWA-HIF-18-062*. McLean, VA: Federal Highway Administration.
- Agrawal, A., Xu, X., & Chen, Z. (2011). *Bridge vehicle impact assessment*. New York, NY: New York State Department of Transportation, University Transportation Research Center.
- Aly, A., & Hoffmann, M. (2022). A case study of protecting bridges against overheight vehicles. *Steel and Composite Structures*, 165-183.
- Atahan, A., Bonin, G., & M., K. (2007). Development of a 30000 kg Heavy Goods Vehicle for LS-Dyna Applications. *International Journal of Heavy Vehcile Systems*, 1-19.
- Cao, A., Agrwal, A., El-Tawil, S., Xu, X., & Wong, W. (2019). Heavy truck collision with bridge piers: Computational simulation study. *Journal of Bridge Engineering*.
- Cao, R., Agrawal, A., El-Tawil, S., & Waider, W. (2021). Data filtering in vehicle-bridge impact simulations: Evaluation of different force filtering methods and recommendations. *Jounral of Bridge Engineering*.
- Cao, R., Agrawal, A., El-Tawil, S., & Wong, W. (2020). Numerical studies on concrete barriers subject to MASH truck impactor. *Journal of Bridge Engineering*.
- Cao, R., Agrawal, A., El-Tawil, S., & Wong, W. (2021). Overheight impact on bridges: A computational case study of the Skagit River bridge collapse. *Engineering Structures*.
- Cao, R., Zuo, X., Agrwal, A., El-Tawil, S., ASCE, F., & Wong, W. (2023). Evaluating the Performance of Protection Beams Subject to Overheight Vehicular Impacts Using Analytical and Machine Learning-Based Methods. *Journal of Bridge Engineering*, 1-14.
- CEN. (2006). *Eurocode 1: Actions on Structures- Part1-7: General Actions-Accidental Actions*. Brussels: European Committee for Standardization.
- Chen, W., Hao, H., & Chen, S. (2015). Numerical analysis of prestressed reinforced concrete beam subjected to blast loading. *Mater. Des.*, 662-674.

- Cheng, S., & Qiao, P. (2015). Numerical Analysis of Honeycomb Sandwich Collision Protection Systems for RC Beams. *Earth and Space*, 536-543.
- Chung, C., Lee, J., & Gil, J. (2014). Structural performance evaluation of a precast prefabricated . *Structure and Infrastructure Engineering*, 777-791.
- Das, S., Brenkus, N., & Tatar, J. (2022). Strategies for Prevention, Protection, and Repair of Bridge Girders Vulnerable to Over-height Vehicle Impacts: A State of the Art Review. *Structures*, 514-533.
- Dyrkolbotn, S. (2021). *Shipping container impact with bridge girders*. Stavanger, Norway: University of Stavanger.
- Hao, Y., & Hao, H. (2014). Influence of the concrete DIF model on the numerical predictions of RC wall responses to blast loadings. *Engineering Structures*, 24-38.
- Harries, K., Kasan, J., Miller, R., & Brinkman, R. (2012). *Updated Research for Collision Damage and Repair of Prestressed Concrete Beams*. US: National Cooperative Highway Research Program Transportation Research Board.
- Highways England. (2020). *CD 366 Design Criteria for Collision Protection Beams*. Highways England.
- Hillman, J. (2012). *Hybrid-Composite Beam (HCB) Design and Maintenance Manual*. Jackson Mill, MO: Missouri Department of Transportation, Bridge No. B0439-MO 76 over Beaver Creek .
- Iowa Department of Transportation (IOWADOT), Office of Bridges and Structures. (2016). *Emergency Response Manual for Overheight Collisions to Bridges*.
- Jackson, K. E., Fasanella, E. L., Annett, M. S., & Polanco, M. A. (2012). Material Model Evaluation of a Composite Honeycomb Energy Absorber. *12th International LS-DYNA Users Conference*.
- Jing, Y. (2017). *Experimental and Analytical Study of Dynamic Behavior of Bridge Superstructures Subjected to Overheight Vehicle Collisions*. Knoxville, TN: University of Tennessee Knoxville.
- Jing, Y., Zhang, X., Zhou, Y., Zhao, Y., & Li, W. (2023). Dynamic Response and Impact Force Calculation of PC Box Girder Bridge Subjected to Over-Height Vehicle Collision. *Buildings*, 1-27.
- Lestari, W., & Qiao, P. (2006). Dynamic Characteristics and Effective Stiffness Properties of Honeycomb Composite Sandwich Structures for Highway Bridge Applications. *Journal of Composites for Construction*, 148-160.
- Lestari, W., Qiao, P., & ASCE, M. (2006). Dynamic Characteristics and Effective Stiffness Properties of Honeycomb Composite Sandwich Structures for Highway Bridge Applications. *Journal of Composites for Construction*, 148-160.
- Li, G., Zhang, C., Wang, D., & Zhang, H. (2005). Study on Live Load Parameter for Highway Bridge. *Journal of Zhengzhou University (Engineering Science)*, 20-23.
- Liu, G. (2012). *Behavior of Bridge Piers during Vehicular Impacts*. New York, NY: City College of New York, City University of New York.

- Livermore Software Technology. (2021). *LS-Dyna Keyword User's Manual: Volume II Material Models*. Livermore, CA: Livermore Software Technology.
- Meirovitch, L. (1967). *Analytical Methods in Vibrations*. New York, NY: Macmillan.
- Miele, C., Plaxico, C., Kennedy, J., Simunovic, B., & Zisi, N. (2005). *Heavy vehicle-infrastructure asset interaction and collision*. U.S. Department of Transportation, Federal Highway Administration, Turner-Fairbank Highway Research Center.
- Miele, C., Plaxico, C., Stephens, D., & Simunovic, S. (2010). *Enhanced Finite Element Analysis Crash Model of Tractor-Trailers (Phase C)*. Knoxville, TN: National Transportation Research Center.
- Miyamoto, A., & King, M. (1994). Modeling of Impact Load Characteristics for Dynamic Response Analysis of Concrete Structures. *Transactions on the Built Environment*, 1743-3509.
- Nemec, N. (2013). *Designing Bridges for Vehicular Collisions*. Texas Department of Transportation.
- Oppong, K., Saini, D., & Behrouz, S. (2021). Characterization of impact-induced forces and damage to bridge superstructures due to over-height collision. *Engineering Structures*.
- Ozadagli, A., Moreu, F., Xu, D., & Wang, T. (2020). Experimental Analysis on Effectiveness of Crash Beams for Impact Attenuation of Overheight Vehicle Collisions on Railroad Bridges. *Journal of Bridge Engineering*.
- Plaxico, C., Miele, C., Kennedy, J., Simunovic, S., & Zisi, N. (2008). Enhanced finite element analysis crash model of tractor-trailers (phase A). Knoxville, TN: National Transportation Center.
- Plaxico, C., Miele, C., Kennedy, J., Simunovic, S., & Zisi, N. (2009). Enhanced finite element analysis crash model of tractor-trailers (phase B). Knoxville, TN: National Transportation Research Center.
- Qiao, P., Yang, M., & Mosallam, A. (2004). Impact Analysis of I-Lam Sandwich System for Over-height Collision Protection of Highway Bridges. *Engineering Structures*, 1003-1012.
- Qiao, P., Yang, M., Mosallam, A., & Song, G. (2008). *An Over-Height Collision Protection System of Sandwich Polymer Composites Integrated with Remote Monitoring for Concrete Bridge Girders*. Arkon, OH: Ohio Department of Transportation Office of Research and Development.
- Sha, Y. (2021). *Shipping Container Impact with Bridge Girders*. Stavanger, Rogaland, Norway: University of Stavanger.
- Sharma, H. (2007). *Design of a Bridge Bumper to Protect Bridge Girders Against Collisions of Overheight Vehicles*. College Station, TX: Texas A&M University.
- Sharma, H., & Hurlbaas, S. (2012). Overheight Collision Protection Measure for Bridges. *Structures Congress*, 790-797.
- Sharma, H., Hurlbaas, S., & Gardoni, P. (2008). Development of a Bridge Bumper to Protect Bridge Girders from Overheight Vehicle Impacts. *Computer-Aided Civil and Infrastructure Engineering*, 415-426.

- Shivakumar, K., Elber, W., & Illg, W. (1983). *Prediction of Impact Force and Duration During Low Velocity Impact on Circulat Composite Laminates*. Hampton, VA: NASA.
- Smith, A. (2014). *Bridge Protective Beam Wrap*. Texas Department of Transportation. Retrieved January 24, 2024, from <https://ftp.txdot.gov/pub/txdot-info/brg/webinars/2014-0716/smith.pdf>
- Xu, D., Yuan, X., Ozdagli, A., Agüero, M., Nasimi, R., Wang, T., & Morue, F. (2022). Over-height truck collisions with railway bridges: attenuation of damage using crash beams. *Earthquake Engineering and Engineering Vibration*, 237-252.
- Xu, L., Lu, X., Guan, H., & Zhang, Y. (2013). Finite-Element and Simplified Models for Collision Simulation between Overheight Trucks and Bridge Superstructures. *Journal of Bridge Engineering*, 1140-1151.
- Xu, L., Lu, X., Smith, S., & He, S. (2012). Scaled model test for collision between over-height truck and bridge superstructures. *International Journal of Impact Engineering*, 31-42.
- Xu, X., Cao, R., El-Tawil, S., Agrawal, A., & Wong, W. (2019). Loading Definition and Design of Bridge Piers Impacted by Medium-Weight Trucks. *Journal of Bridge Engineering*.
- Yang, M. (2006). *Impact Mechanics of Elastic and Elastic-Plastic Sandwich Structures*. Arkon, OH: The University of Arkon.
- Yang, M., & Qiao, P. (2008). Quasi-static crushing behavior of aluminum honeycomb materials. *Journal of Sandwich Structures & Materials*, 133-160.
- Yang, M., & Qiao, P. (2010). Analysis of Cushion Systems for Impact Protection Design of Bridges Against Overheight Vehicle Collision. *International Journal of Impact Engineering*, 1220-1228.